ANALYSIS OF RADIAL ARTERIAL PULSE WAVEFORM

A dissertation submitted in partial fulfillment of the requirements

for the degree of

Master of Technology

by

Aparna M. Surve

(*Roll No. 01307901*)

under the supervision of

Prof. P. C. Pandey

Department of Electrical Engineering

Indian Institute of Technology, Bombay

Powai, Mumbai 400 076

January 2004

Indian Institute of Technology, Bombay

DISSERTATION APPROVAL

Dissertation entitled: **Analysis of Radial Arterial Pulse Waveform**

by **Aparna M. Surve**

is approved for the award of the degree of **MASTER OF TECHNOLOGY in Electrical Engineering** with specialization of **Control and Instrumentation**.

Supervisor	______________________	(Prof. P. C. Pandey)
Internal Examiner	______________________	(Prof. V. M. Gadre)
External Examiner	______________________	(Dr. V. K. Madan)
Chairperson	______________________	(Prof. R. Manchanda)

Date:

Acknowledgement

I would like to express my deepest gratitude to my guide Prof. P.C. Pandey for guidance, support, and encouragement throughout the course of this project. I would like to thank Prof. T. Anjaneyulu for the suggestions I have received from him.

I am thankful to Parveen Lehana, Piyush Desai, N. S. Manigandan, Juhi Khanna and Vinod Pandey for their help in recording of signals required during investigation. I would also like to extend my sincere thanks to my colleague Santosh Pratapwar and Mr. V. Kamble of our laboratory for all the help and support during this project.

Aparna M. Surve

January 2004

Aparna M. Surve / Prof. P.C. Pandey (supervisor): "Analysis of radial arterial pulse waveform", *M.Tech. dissertation*, Department of Electrical Engineering, Indian Institute of Technology, Bombay, January 2004.

Abstract

Noninvasive recording of pressure pulse waveform from radial artery can be used for obtaining valuable diagnostic information, by analyzing it for temporal characteristics, spectral characteristics and its cross-correlation with phonocardiogram and ECG. The pulse waveform can be obtained by the transducer of electronic stethoscope or phonocardiograph as well as a piezoelectric transducer. The pulse waveform obtained using phonocardiograph sensor is found to be noisy, and further processing needed signal enhancement. Spectral subtraction method, reported earlier for enhancement of noisy speech, was used for enhancement of pulse signal. The noise spectrum is estimated using a noise recording from a nearby site, and it is used during the entire duration of signal to be enhanced. Next, quantile-based estimate of noise spectrum from the noisy pulse waveform itself is used for continuous updating of noise spectrum for spectral subtraction. The effect of physical exercise on the pulse waveform and its cross-correlation with phonocardiogram is studied.

Contents

List of symbols

Symbol	Explanation
K	Spring constant
F_1	Hold-down force
P_a	Foot of pulse
P_b	First shoulder
P_c	Second shoulder
P_d	Incisura
θ	Angle of deviation of percussion wave
f_s	Sampling frequency
$S(f)$	Spectral energy density
V_{max}	Maximum amplitude
V_{th}	Clipping level
α	Subtraction factor
β	Spectral floor factor
T	Averaging duration

List of abbreviations

Symbol	Explanation
ADC	Analog-to-digital converter
MAP	Mean arterial pressure
MSP	Mean systolic pressure
MDP	Mean diastolic pressure
Sa/s	Samples/second
SER	Spectral energy ratio
PSG	Pulse spectral graph
PCG	Phonocardiogram
T_m	"Medetron" stethoscope
T_s	"Stethmate" stethoscope
DSO	Digital storage oscilloscope
PC	Personal computer
FIR	Finite impulse response
BPF	Band pass filter
FFT	Fast Fourier transform
IFFT	Inverse fast Fourier transform
S.D.	Standard deviation
ABNE	Average-based noise estimation
QBNE	Quantile-based noise estimation
RMS	Root mean square
bpm	Beats per minute

List of figures

List of tables

Chapter 1
Introduction

1.1 Background

Noninvasive recording of pressure pulse waveform from the radial artery can be used for obtaining valuable diagnostic information, by analyzing it for temporal characteristics, spectral characteristics, and its cross-correlation with phonocardiogram and ECG. In most traditional systems of medicine, e.g. *nadishastra* (a branch of *ayurveda*, ancient and well established medical system of India), sensing of arterial pulse pressure forms an essential part of diagnosis. Normally physician' s palm supports the patient' s wrist and pulse examination is carried out using finger tips [1][2][3]. The diagnosis requires a long period of study and practice by the individual physician, without the benefit of any physical recordings and analysis aids.

Early studies on pulse waveform have used Dudgeon' s sphygmograph [3][4]. Its use involved a tedious process of preparation of tracings and measurements from the tracings. Further, it had other limitations like poor dynamic response. Several instruments have been developed and reported for sensing the pulse waveform and giving the output as an electrical analog voltage or as digitized samples and built-in analysis [5][6][7][8][9][10][11].

1.2 Project objective

Recording of pulse waveform using the transducer of an electronic stethoscope or phonocardiograph has been investigated. The main advantage of this technique is a good dynamic response. But the transducer has relatively poor low frequency response. The signal is corrupted by noise, environmental sounds as well as the vibrations from various smaller blood vessels. The objective of this project is to use pulse sensing and investigate signal processing methods for obtaining clean pulse waveform for its analysis. As the noise has essentially the same band as the signal, it cannot be reduced by filtering techniques. Hence the spectral subtraction method, generally used for enhancement of noisy speech, is used for noise reduction in the pulse waveform. For this purpose, estimate of noise spectrum can be obtained using noise recording from a nearby site or by using a quantile based spectral estimate of noise from the noisy pulse waveform itself. Compared to phonocardiograph sensor, relatively better pulse waveform is obtained by using piezoelectric transducer. Cross-correlation of the pulse waveform with phonocardiogram has been investigated for change in the delay in the cross-correlation peak as an indication of change in arterial blood flow rate.

1.3 Dissertation outline

The different sensors used for acquisition of pulse waveform along with the analysis of pulse waveform are discussed in Chapter 2. Chapter 3 describes the experimental set up used for investigation. The pulse waveform obtained by using phonocardiograph is noisy and Chapter 4 provides a description of the various signal enhancement techniques, including band-pass filtering and centre-clipping method and spectral subtraction method using averaged and quantile-based noise estimation (QBNE). The effect of physical exercise on the pulse waveform is presented in the Chapter 5. Chapter 6 gives summary of the work carried out and scope for future work

.

Chapter 2
Acquisition and analysis of pulse waveform

In *nadishastra* based diagnosis, three fingers are used as sensors. Several sensors giving electrical output have been reported. Some of these are described here. This chapter also presents a review of the analysis of the pulse waveform.

2.1 Dudgeon's sphygmograph

In 1882, Dudgeon designed sphygmograph for measuring blood pressure from the radial artery at the wrist as shown in Fig 2.1 [3][4]. The instrument is made of a starter on its upper surface, two pulleys at the two ends of a small rotatory bar, a freely hanging needle and a key which is set in the back of the body of the instrument. The instrument is used for pulse tracing by rotating key in anticlockwise direction. A rectangular piece of smoked paper is fitted in between the two pulleys for pulse wave recording. When the starter is set, pulleys start working by rotating the small bar. Thus the smoked paper is moved forward and pulse tracing is done by means of the hanging needle. Dudgeon' s sphygmograph was used by Upadhyay [3] for obtaining pulse tracings and quantitative measurements for pulses classified in accordance with *nadishastra*. Fig 2.2 shows some sample pulse tracings.

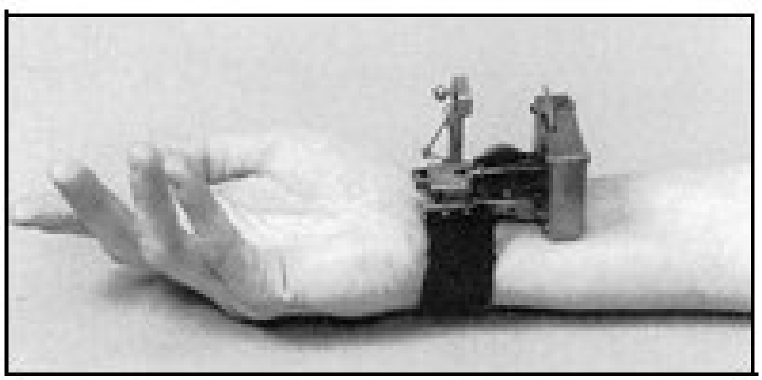

Fig 2.1 Dudgeon' s sphygmograph [4]

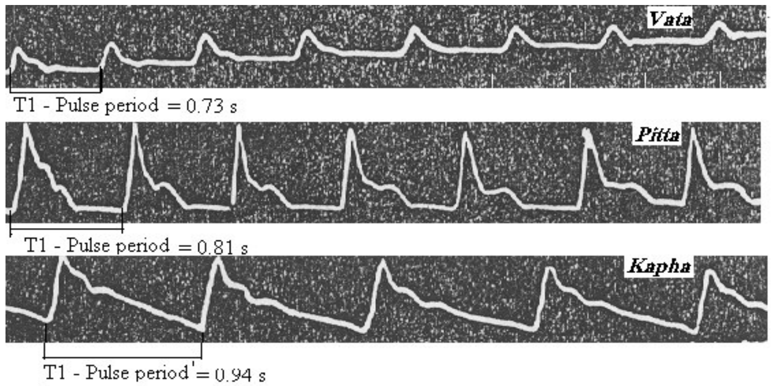

Fig 2.2 Pulse tracings using Dudgeon's sphygmograph as obtained by Upadhyay [3]

2.2 Arterial tonometer

The arterial tonometer is an instrument used for measuring arterial blood pressure. Typically, it is placed over a superficial artery e.g., the radial artery on the wrist [5]. Fig 2.3 shows the schematic diagram of simple arterial tonometer sensor. The sensosr assembly is held by a strap with hold-down force of F_1. The tonometer sensor is modeled as an assembly of springs with spring constant K. The arterial rider senses arterial pressure. Side structure allows the sensor to rest on the arterial wall. Design of sensor is based on following assumptions [5].

- The artery above which sensor is placed is supported from below by bone (e.g. the radial artery is supported by radial bone) and the thickness of the skin over the artery is insignificant compared to the diameter of the artery.
- The arterial rider as shown in Fig 2.3 is smaller than the flattened area of the artery, and is placed over the flattened area of artery. It is about 0.2 mm wide.
- The spring constant K of the force transducer is large as compared to the effective spring constant of the artery.

Recording of pulse signal is done by adjusting appropriate hold down force F_1. The procedure involves increasing the hold-down force and simultaneously pulse signal is recorded as shown in Fig 2.4. The pulse amplitude slowly increases as shown in part A, becoms maximum as shown in part B, further reduces in part C, irrespective of any increase in F_1. Hence F_1 used for acqusition of pulse signal as shown in part B, is selected as optimum hold-down force. The tonometer sensor uses strain gage transducer, semiconductor pressure transducer, or a capacitive transducer [5][10]. Fig 2.5 shows the block diagram of the strain gage based tonometer sensor. Strain gages (gage factor = 110) are attached to miniature diaphragm supporting the arterial rider of area 0.25" × 0.065". Side plates are integral part of the transducer body. The pressure in the air chamber is controlled by a pressure regulator. Straps are attached to the air chamber. The pulse amplitude increases with increase in pressure in the air chamber up to a certain value, and thereafter it reduces irrespective of any increase in pressure. The pulse waveform obtained by using strain gage based tonometer sensor is as shown in Fig 2.6. The signal output 10.4 μV per mmHg, with 4 V excitation to strain gage bridge circuit [10].

An arterial rider present in simple tonometer requires accurate placement over the superficial artery, hence requires a skilled operator. A multiple-element arterial tonometer sensor [5] is shown in Fig 2.7. It consists of an array of minimum 25 arterial riders with interelement spacing of about 0.2 mm [5]. The sensor requires precise positioning over the artery such that some elements of the array are centered over the artery. Then a computer automatically selects the sensor element that is correctly positioned over the artery for acquisition of pulse pressure. It searches for the largest pulse amplitude, the corresponding sensor element will then be chosen for further acquistion. Multiple-element tonometer sensor uses piezoresistive strain gages attached to diaphragm of 10 μm thick [5]. Some of the sensors based on arterial tonometry principle are described here.

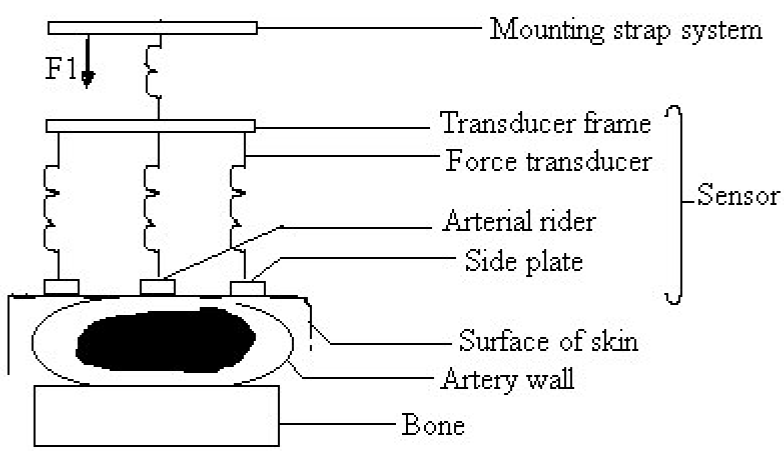

Fig 2.3 Schematic diagram of simple arterial tonometer [5]

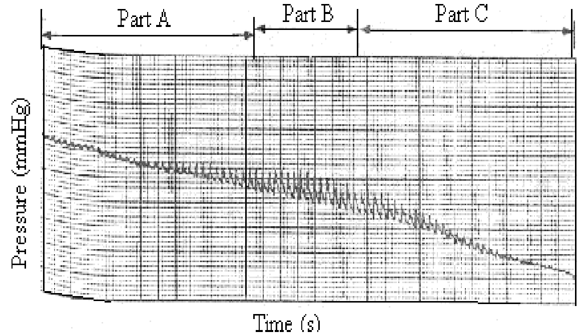

Fig 2.4 Procedure for obtaining optimal hold-down force in simple tonometer [5]

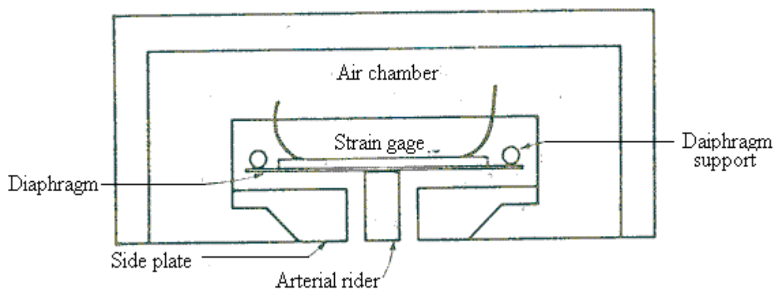

Fig 2.5 Strain gage based tonometer sensor [10]

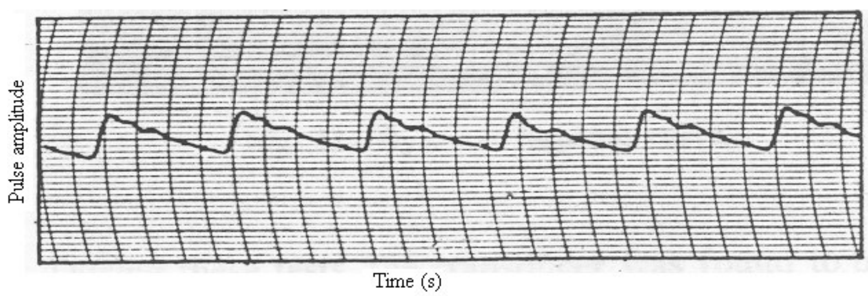

Fig 2.6 Pulse signal obtained by using strain gage based tonometer sensor [10]

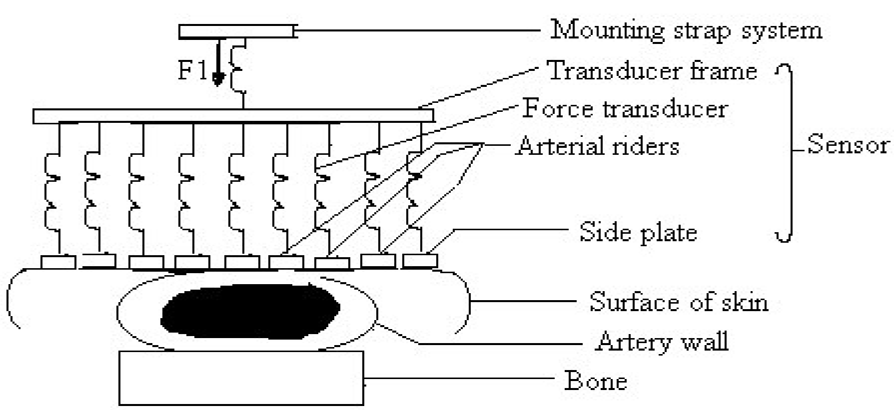

Fig 2.7 Schematic diagram of multiple-element arterial tonometer [5]

"MediWatch" is a recently reported [6][7] non-invasive device designed to continuously monitor the blood pressure and pulse rate. It comprises of the sensor system, the strap system and the watch head as shown in Fig 2.8, it has a pressure sensor housed in a special casing, which contains a plunger that is ' free-floating' as it applanates the radial artery. The strap provides constant force for effective applanation and ensuring the position of the sensor housing to remain constant after any wrist movement as shown in Fig 2.9. Change in the electrical signals due to change in pressure is detected as a result of the piezoresistive nature of the sensor and coupled to the watch head via three small cables along the strap. The arterial pulsations are captured as digitized with a sampling rate of 32 Sa/s and analyzed [6]. MediWatch provides continuous beat-to-beat wrist arterial pulse rate measurements such as heart rate, systolic and diastolic blood pressure (range = 10 to 300 mmHg), mean arterial pressure and pulse pressure. The sensitivity of MediWatch is reported to be consistent in both the low and high pressure conditions [7]. Fig 2.10 shows the sample pulse waveform obtained by using MediWatch.

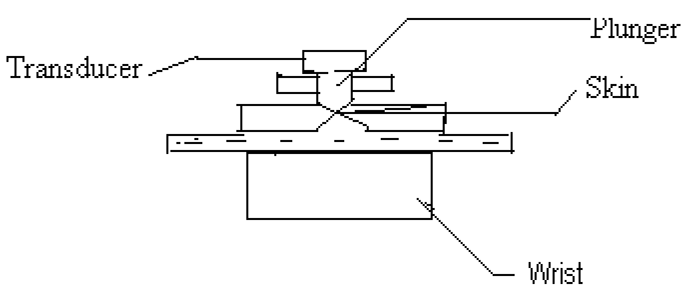

Fig 2.8 Pulse sensor "MediWatch" [7]

Fig 2.9 Top view of MediWatch [7]

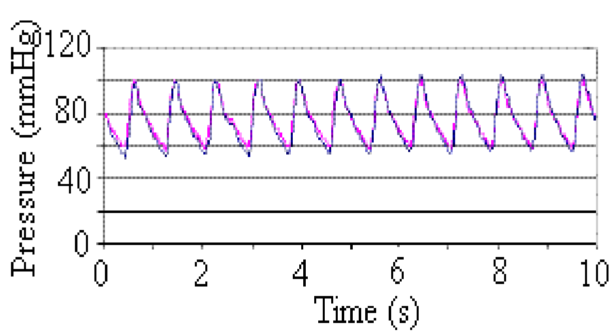

Fig 2.10 Pulse waveform obtained by MediWatch [7]

"Model 7000" is developed by Colin Medical Instruments Corp [8] for providing beat-to-beat blood pressure values with arterial pressure waveform. Fig 2.11 shows its working. This sensor contains array of piezoelectric pressure transducers of length 0.2 mm and separated by 0.2 mm. The sensor is placed on the wrist over the radial artery. A pneumatic pump and bellows press the transducer array against the skin and tissue above an artery. This pressure is known as the hold-down pressure. To determine optimal hold- down pressure, the monitor searches through a range of pressure values until it measures the largest pulse pressure value, the procedure is as shown in Fig 2.12. When the artery is partially flattened, a graph called tonogram, can be plotted to show the pulse amplitude versus transducer number. The sensor element whose pulse amplitude is near the maximum pulse amplitude is calibrated to the systolic and diastolic values obtained in the oscillometric cuff measurement and used for pulse acquisition.

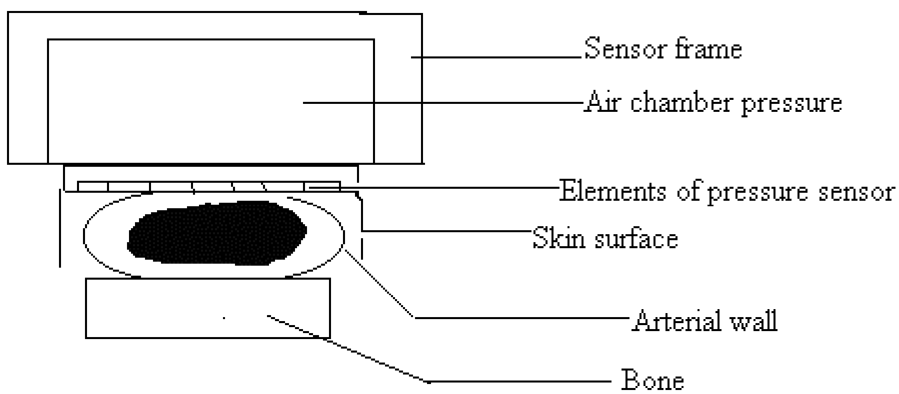

Fig 2.11 Sensor used in Model 7000 [8]

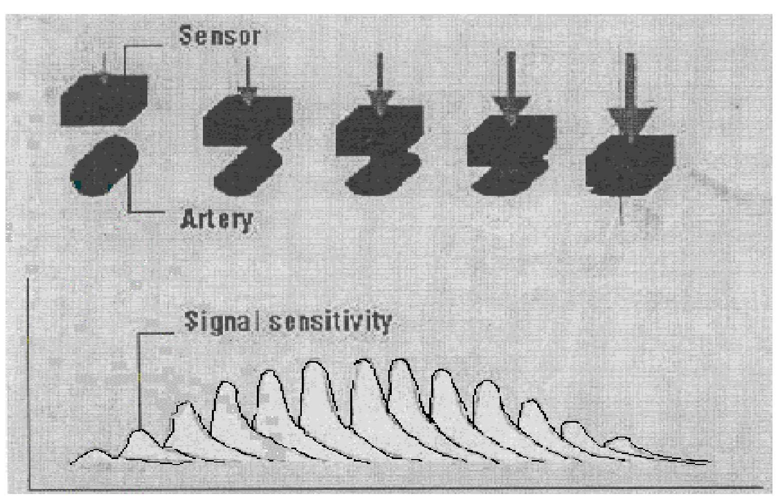

Fig 2.12 Procedure for obtaining optimal hold-down pressure in Model 7000 [8]

2.3 Force transducer based sensor

Sudheer Shah implemented a blood pressure measurement system based on a capacitive transducer, as part of his M.Tech. dissertation at IIT Bombay [11]. The block diagram of the system is as shown in Fig 2.13a. The sensor converts arterial force into displacement and the displacement into an electrical signal. Fig 2.13b shows a schematic of the capacitive transducer, which was used for sensing the arterial deflection. The capacitance between 1 and 2 is the capacitance of the main transducer. The capacitance between 1 and 3 and 2 and 3 are fixed and small. Fig 2.13c shows a sectional view of the transducer. The capacitor is made of a deflectable corrugated diaphragm and a fixed electrode. The deflectable diaphragm is made of Phosphor Bronze, parallel planes with clamped edges. The fixed electrode is made of stainless steel and has a plane surface parallel to the undeflected diaphragm across an air gap. The diaphragm is stuck with the rider at its center. For free movement of rider, a narrow gap is kept between it and the other side structure. A perspex ring is used for providing insulation of the electrode from the side structure. The side structure and rider, come into contact with the body. In between the fixed electrode and diaphragm, a thin mylar sheet of 25 microns is kept for providing insulation between the diaphragm and the side structure. By using the nylon strap, the transducer was tied to wrist, on the radial artery and the blood pressure waveform was obtained which is shown in Fig 2.13d.

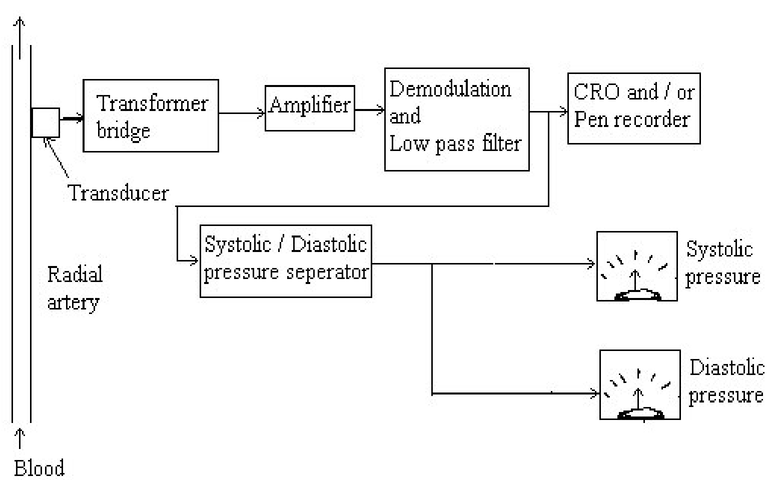

Fig 2.13a Block diagram of blood pressure monitoring system [11]

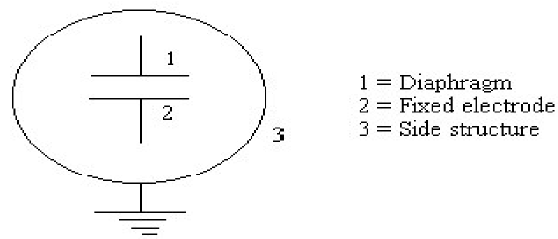

Fig 2.13b Electrode capacitor [11]

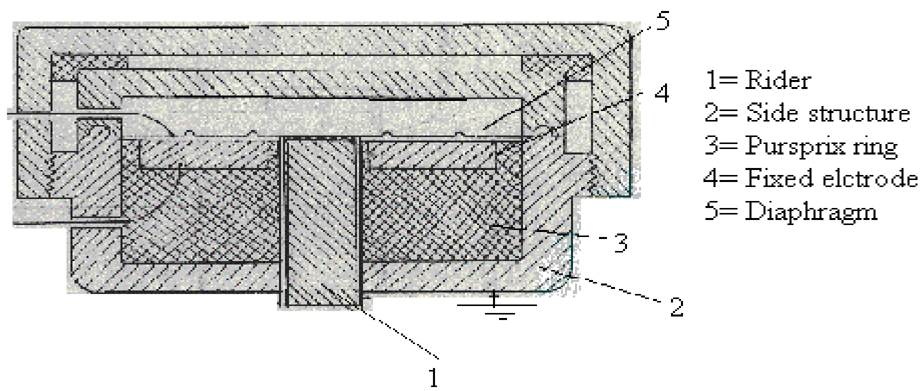

Fig 2.13c Transducer assembly [11]

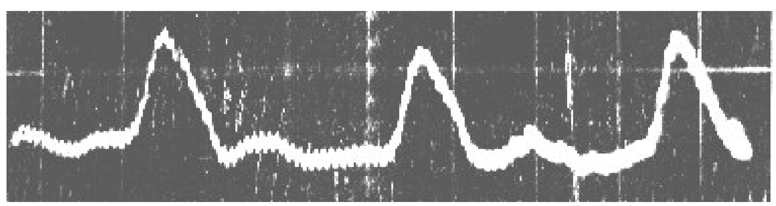

Fig 2.13d Blood pressure waveform sensed by transducer [11]

2.4 Microphone based system

Binghe and Jinglin [9] and Lee and Wei [12] have reported a microphone based system for detecting pulse signal from the radial artery, which is as shown in Fig 2.14. It is composed of the sound-coupling cavity, condenser microphone (B&K- 4147), preamplifier (B&K- 2639), microphone power supply (B&K- 2804) and the data recorder. The condenser microphone was used as a transducer to convert pulse on the wrist into electrical signals. The microphone used has 0.5" diameter with a flat frequency response in the range of 0.1 Hz to 20 kHz. It was tightly sleeved into a Teflon tubing, whose opening was about 5 mm from the diaphragm of the microphone. The sleeve opening was put in direct contact with the skin of the wrist at the specific position [12]. The pulse in the artery is transmitted through the tiny enclosed air space onto the diaphragm of the microphone and outputted as an electrical signal, and the analog waveform is digitized for further analysis. The power spectra of four different types of pulses: normal pulse, smooth pulse, wiry pulse and slow-intermittent pulse, obtained by using the microphone based system are as shown in Fig 2.15.

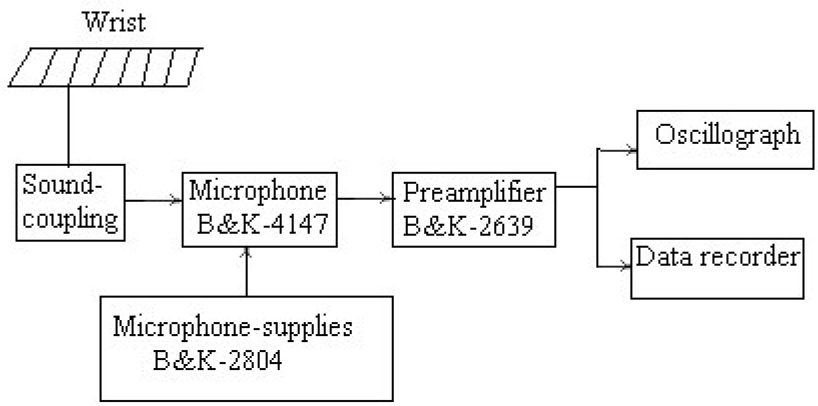

Fig 2.14 Microphone based pulse sensing system for pulse signal, reported by Binghe and Jinglin [9]

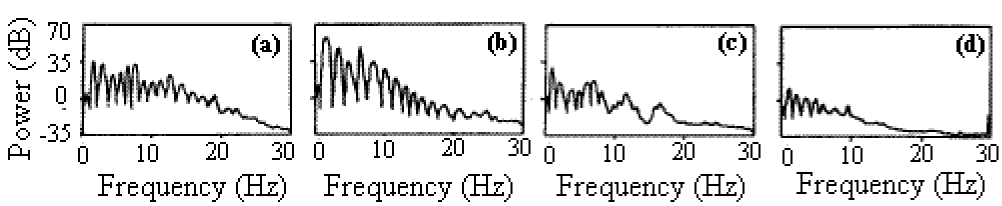

Fig 2.15 Power spectra of pulse signals (a) normal pulse (b) smooth pulse (c) wiry pulse (d) slow-intermittent pulse [9]

2.5 Analysis of pulse waveform

Upadhyay [3] used Dudgeon' s sphygmograph for pulse sensing and quantitative measurements. The pulse wave was obtained for a large number of normal subjects as well as patients at different time duration during the day. The analysis of pulse waveform involved study of following parameters [3].

- Pulse period (time taken by each pulse wave).

- Length of percussion wave from the point of its start to the highest point of its top, which represents the amount of pressure exerted on the blood flow due to the contraction of left ventricle.
- Distance between two nearest top points of the wave. It is due to rate of contraction of left ventricle.
- Angle of deviation of percussion wave.
- Distance of dicrotic notch from the base line.

According to *ayurveda*, by using *nadishastra* technique, one can predict about the three *doshas*: *vata*, *pitta* and *kapha* in the body [1][2]. Upadhyay studied the above parameters for pulse waves with the three *doshas*. Fig 2.16a, Fig 2.16b and Fig 2.16c shows the sample pulse wave obtained from normal subjects with *vata*, *pitta* and *kapha dosha* respectively. Table 2.1 shows the measurements of parameters corresponding to *vata*, *pitta* and *kapha* pulses of sample recording.

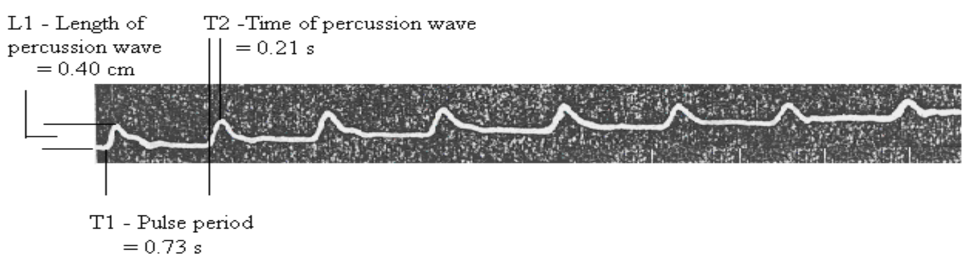

Fig 2.16a *Vata* Pulse obtained using Dudgeon' s sphygmograph [3]

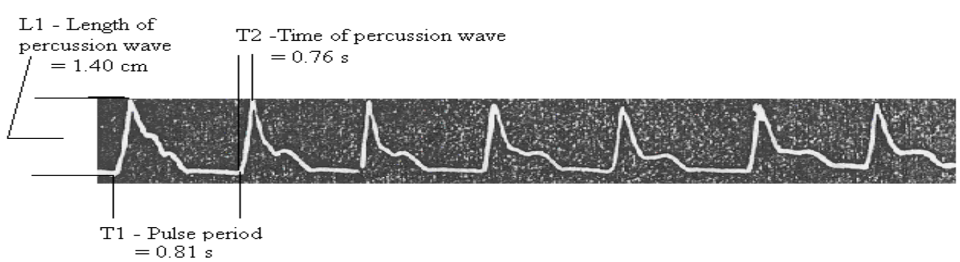

Fig 2.16b *Pitta* Pulse obtained using Dudgeon' s sphygmograph [3]

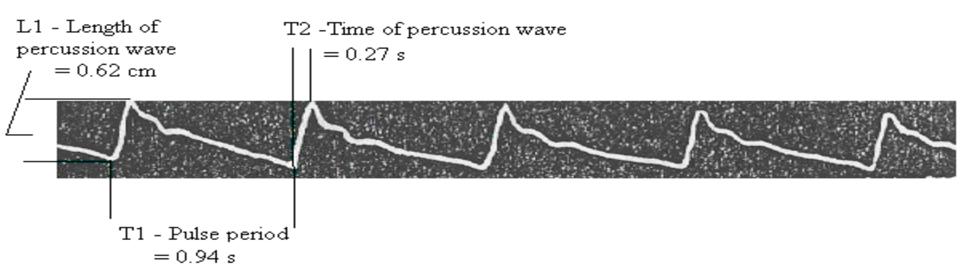

Fig 2.16c *Kapha* Pulse obtained using Dudgeon' s sphygmograph [3]

Table 2.1 Measurements on *vata*, *pitta* and *kapha* pulses [3]

Type of pulse	Pulse period (s)	Length of percussion wave (cm)	Time of percussion wave (s)	Angle of deviation (°)	Distance of dicrotic notch (cm)
Vata	0.73	0.40	0.21	65°	0.15
Pitta	0.81	1.40	0.76	81°48'	0.8
kapha	0.94	0.62	0.27	77°30'	0.30

From Table 2.1, the *vata* pulse takes minimum pulse period and has smallest length of percussion wave. It has least angle of deviation and minimum distance of dicrotic notch from the base line of pulse wave. The *pitta* pulse has medium pulse period, highest length of percussion wave, maximum deviation of angle in bending towards the base and maximum distance of dicrotic notch from the base line of pulse wave. The *kapha* pulse indicates maximum pulse period, medium length of percussion wave, medium deviation of angle in bending towards the base and medium distance of dicrotic notch from the base line.

Dasrao et al [6] used Mediwatch for pulse sensing and measurement of arterial pulse rate, systolic and diastolic blood pressure. An acquired pulse waveform is as shown in Fig 2.17. At the beginning of the cycle, the minimum pressure P_a, foot of pulse occurs at time T_a. The pulse waveform rises from minimum pressure till the first peak where it forms a first shoulder with pressure P_b at time T_b and proceeds to a second shoulder with pressure P_c at time T_c. Further pulse wave decreases with a notch P_d, incisura at time T_d, after which pulse wave decreases gradually. P_a indicates diastolic pressure, which rises corresponding to the onset of systole. P_b occurs due to maximum blood flow during systole and P_c represents systolic pressure. P_d corresponds to the closure of aortic valve. Based on these parameters, the arterial system of subject was described which involved following parameters [6].

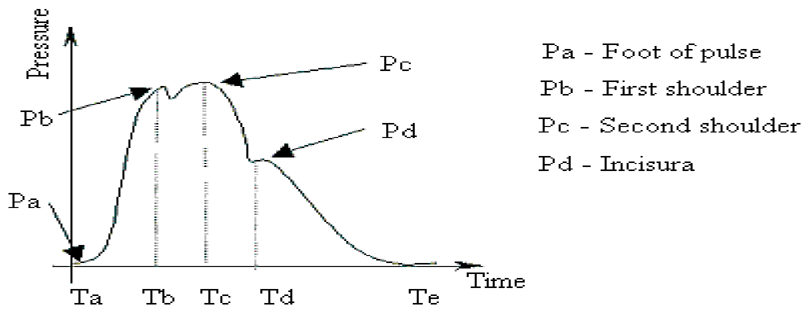

Fig 2.17 Pulse wave analysis using MediWatch [6]

- Augmented pressure is defined as the pressure difference between the first peak, P_b and second peak, P_c.
- Systolic (tension) pressure time index is the integral of pressure multiplied by time throughout systole.
- Diastolic pressure time index is the integral of the diastolic part of the pressure wave.
- Sub-endocardial viability ratio is the ratio of diastolic pressure time index to systolic pressure time index.
- Pulse pressure is the pressure difference between the systolic pressure P_c and end-diastolic pressure $P_{a.}$
- Mean arterial pressure is the area under curve of a whole pulse wave cycle divided by time period of cycle.

$$MAP(mmHg) = \frac{\sum_{j=T_a}^{T_e} P_j}{T}$$

where T = time period of pulse wave (T_e - T_a)

- Mean systolic pressure is the average pressure between the foot of pulse, P_a and incisura, P_d.

$$MSP(mmHg) = \frac{\sum_{j=T_a}^{T_d} P_j}{T_d - T_a}$$

- Mean diastolic pressure is the average pressure between the incisura, P_d and beginning of next pulse wave.

$$MDP(mmHg) = \frac{\sum_{j=Td}^{T_e} P_j}{T_e - T_d}$$

MediWatch is used for ambulatory pressure monitoring [6][7], in which continuous blood pressure readings are taken during the patient' s normal daily activities. The blood pressure readings for whole day are obtained and plotted which gives the indication of type of blood pressure pattern [6][7]. Fig 2.18a shows normal blood pressure pattern. The normal blood pressure pattern falls within the range [7] as given in Table 2.2. Isolated systolic hypertension pattern is as shown in Fig 2.18b. It shows high systolic blood pressure (BP) while diastolic BP remains normal. Nocturnal hypertension is as shown in Fig 2.18c. It has day-time BP in normal range but night-time BP increases.

Table 2.2 Blood pressure range for normal subject [7]

BP	**Day-time range** (mmHg)	**Night-time range** (mmHg)
Systolic	115 to 140	95 to 125
Diastolic	65 to 90	55 to 75

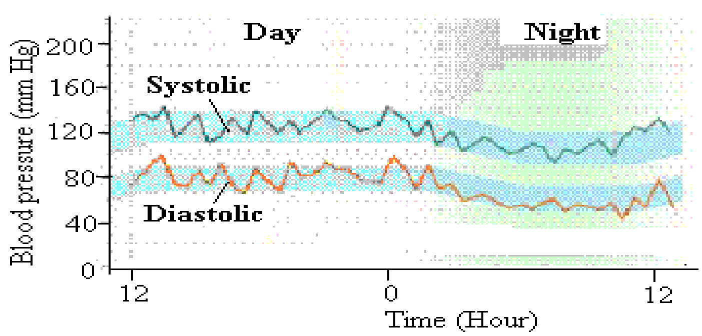

Fig 2.18a Normal blood pressure pattern obtained by using MediWatch [6]

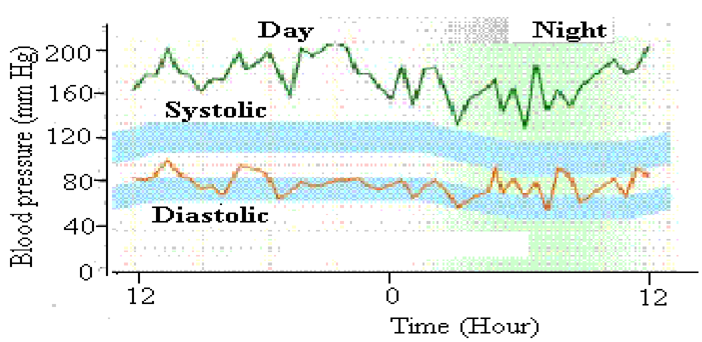

Fig 2.18b Isolated systolic hypertension pattern obtained by using MediWatch [6]

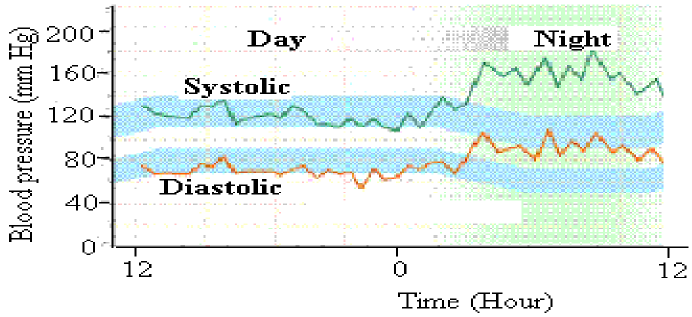

Fig 2.18c Nocturnal hypertension pattern obtained by using MediWatch [6]

Binghe and Jinglin [9] have used the microphone based pulse detecting system for sensing arterial pulse at wrist and analyzed the power spectra of four types (according to traditional Chinese medicine system) of pulses. The pulse has been classified as normal pulse, smooth pulse, wiry pulse and slow-intermittent pulse [9]. The pulse signal was low pass filtered with cut-off frequency 50 Hz. Further analog pulse signal was digitized by using sampling frequency f_s of 128 Sa/s with a sampling length T of 16 s. The power spectrum of pulse signal was obtained by using FFT length of 2048 ($= f_s\ T$) as shown in Fig 2.19.

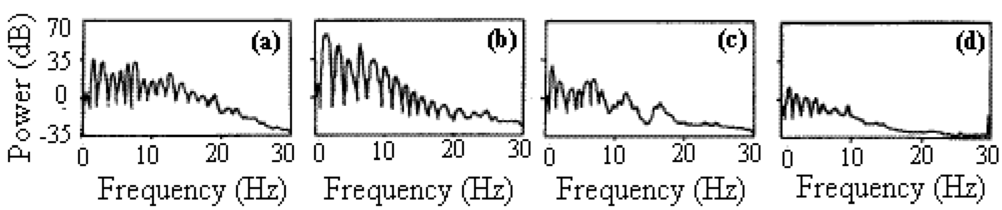

Fig 2.19 Power spectra of pulse signals (a) normal pulse (b) smooth pulse (c) wiry pulse (d) slow-intermittent pulse [9]

Power spectra show that spectral density extends up to 25 Hz, with the envelope decreasing with increase in frequency. The spectral energy of pulse is approximately concentrated below about 10 Hz. Hence the spectral energy within 10 Hz, total energy was obtained by integrating the energy over 0 Hz-10 Hz and 0 Hz-40 Hz respectively. The spectral energy ratio (*SER*) of the normal pulse within 10 Hz was above 99% of the total energy, the corresponding values for wiry pulse and smooth pulse were 97% and 83.7% respectively.

Lee and Wei [12] analyzed the spectrum of pulse at radial artery at wrist and correlated its spectral features with health condition of subject. In traditional Chinese medicine, the pulse is sensed at three different points: *Tsun*, *Guan* and *Chy* along the radial artery on the wrist of both hands [12]. By applying maximum and minimum pressure at these three points, physician detects the condition of the internal organs of the patient as indicated in Fig 2.20.

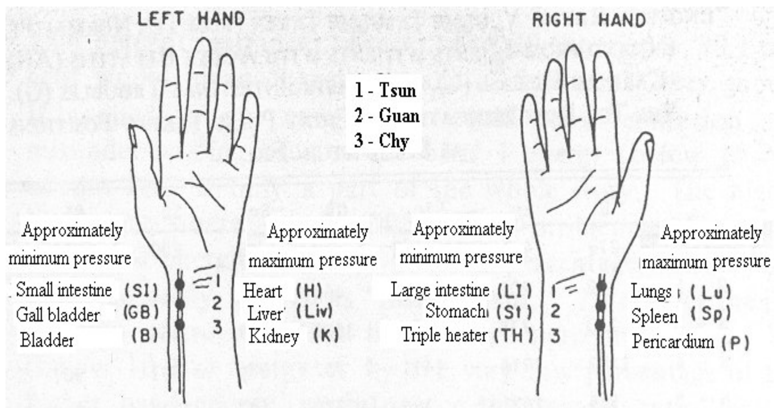

Fig 2.20 Position for pulse sensing used in traditional Chinese medicine [12]

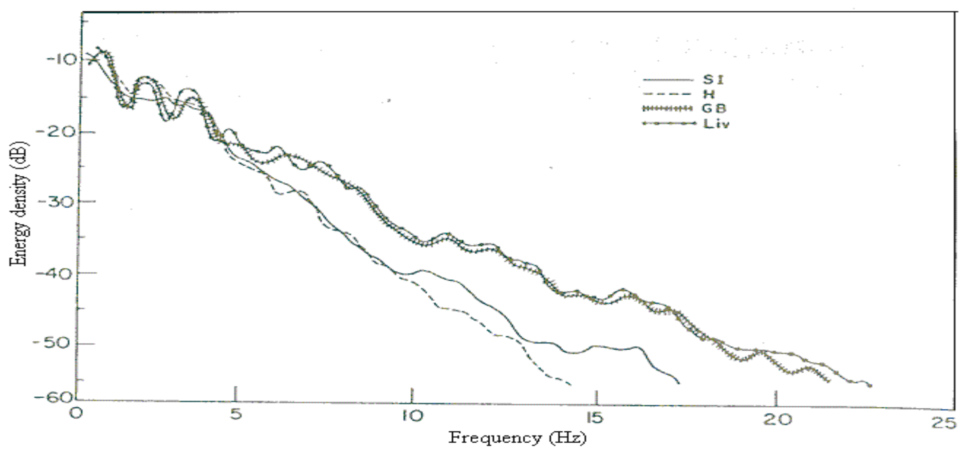

Fig 2.21 Pulse spectral graphs for the pulses obtained from the left wrist of normal subject by using condenser microphone ("Bruel & Kjar 4147") [12]

By keeping the condenser microphone ("Bruel & Kjar 4147") at *Tsun* and *Guan* positions, using approximately minimum and maximum pressure the analog waveforms of pulse were sensed at both the wrist and digitized for its spectral analysis in terms of spectral energy ratio (*SER*). The recording of pulse at *Chy* position was avoided in order to prevent inconvenience to patient by applying pressure to three close points for long duration. *SER* is defined as the ratio of the energy of pulse spectral graph (PSG) below 10 Hz to that above 10 Hz [13].

$$SER = \int_{f=0}^{10} S(f)df \Big/ \int_{f=10}^{50} S(f)df$$

where *S*(*f*) is the spectral energy density.

The PSG of normal subject at two different points: *Tsun* and *Guan* of left hand is as shown in Fig. 2.21. The pulse signal is present in the range of 0 Hz- 25 Hz and decreases gradually. However the energy has been measured from 1 Hz to 50 Hz, assuming the signal below 1 Hz to be due to motion artifact [12]. The power spectra at eight different points are approximately coinciding with each other. It indicates the pulse waveforms taken from all positions are almost similar for normal person [12]. The *SER* values calculated for large number of normal subjects showed that the maximum energy of pulse signal is concentrated below 10 Hz [12].

Chapter 3
Experimental set up

3.1 Introduction

This chapter discusses the experimental set up used for acquisition of pulse signal. For this project, an electronic stethoscope or phonocardiograph, which is normally used for recording of the heart sounds and murmurs, was used. The main advantage of this technique is a good dynamic response. The diameter of the chest-piece (1.5") of phonocardiograph is comparatively larger than the diameter of the radial artery. Hence along with the pulse signal, the noise: environmental sounds and the vibrations from various smaller blood vessels were picked up. Further a piezoelectric transducer (diameter = 0.5") was used for pulse pick up. The obtained pulse waveform was much less noisy as compared to that from the phonocardiograph sensor.

3.2 Pulse pick up using phonocadiograph

In the beginning of this project, it was decided to use an electronic stethoscope or phonocardiograph, which is normally used for recording of the heart sounds and murmurs, which gives diagnostic information about the heart valve actions [14]. The principle instrument clinically used for recording of PCG is the acoustical stethoscope. The stethoscope housing is in the shape of a bell. It makes contact with the skin of chest wall, which serves as the diaphragm at the bell rim [15]. Applied pressure causes displacement of the diaphragm. An improvement over the acoustal stethoscope, which usually has low fidelity, is an electronic stethoscope [14]. It has a microphone, an amplifier and a head set. The commonly used microphones for recording PCG are contact microphone and air coupled microphone. They are further classified into crystal type and dynamic type. The crystal microphones contain a wafer of piezoelectric material, which generates an electrical output when subjected to mechanical stresses due to heart sounds. They are smaller in size and more sensitive. The dynamic type microphone consists of a moving coil having a fixed magnetic core inside it. The coil moves with the heart sounds and gives a voltage output. The amplifier used for PCG has a wide bandwidth with the frequency range from about 20 Hz to 2 kHz. The amplifier usually has a gain compensation circuits [14] to increase the amplification of high frequency signals, which are usually of lower intensity. It is to be noted here that the PCG transducer will act as a differentiator for the pulse signal. It does not record low frequency components properly. However it provides a boosting of high frequency components.

The PCG and pulse waveform were acquired by using two different electronic stethoscopes, "Medetron" and "Stethmate" [16], available phonocardiographic instruments in our lab. Medetron and Stethmate are denoted as Tm and Ts and are made of air-coupled crystal microphone. Both the instruments have two outputs: binaural acoustic output and auxiliary electrical output. From binaural output the sound of the signal, which is being recorded can be heard, by connecting it to ears. We record the auxiliary electrical output through a DSO or the line input of PC sound card. DSO model ("Agilent 54621D") could be used for recording length of 2000 samples and pulse amplitude range of 300-500 mV. PC sound card can be used for very large length recordings. A sampling rate of 11.025 k Sa/s was used (11.025 k Sa/s, followed by 10:1 decimation). The specifications of sound card are given in the Appendix [17][18]. Hence by listening to the sound from the binaural output, the approximate positioning of the chest pieces were done on the chest and at radial artery on the wrist for PCG and pulse waveform respectively. The waveform can be stored in the binary format as 16-bit data [17]. Fig 3.1 shows PCG recorded using Tm and Ts respectively. Magnitude spectra of PCG obtained using Tm and Ts are as shown in Fig 3.2.

(a) PCG using Tm

Voltage range: ± 800 mV

(b) PCG using Ts

Voltage range: ± 500 mV

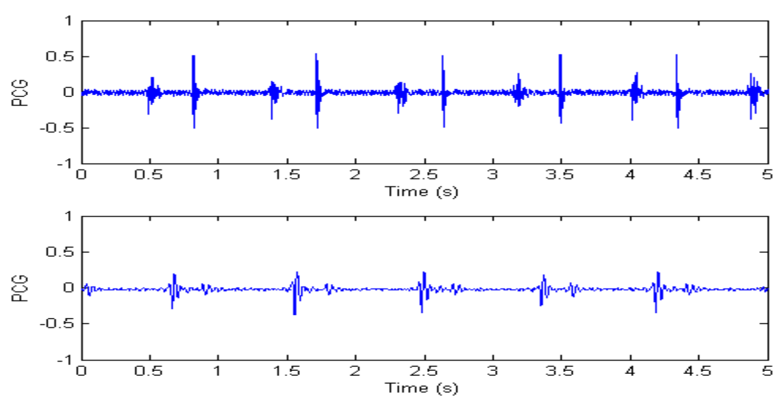

Fig 3.1 PCG recorded using phonocardiograph sensors

(**a**) Spectrum: PCG recorded using Tm

(**b**) Spectrum: PCG recorded using Ts

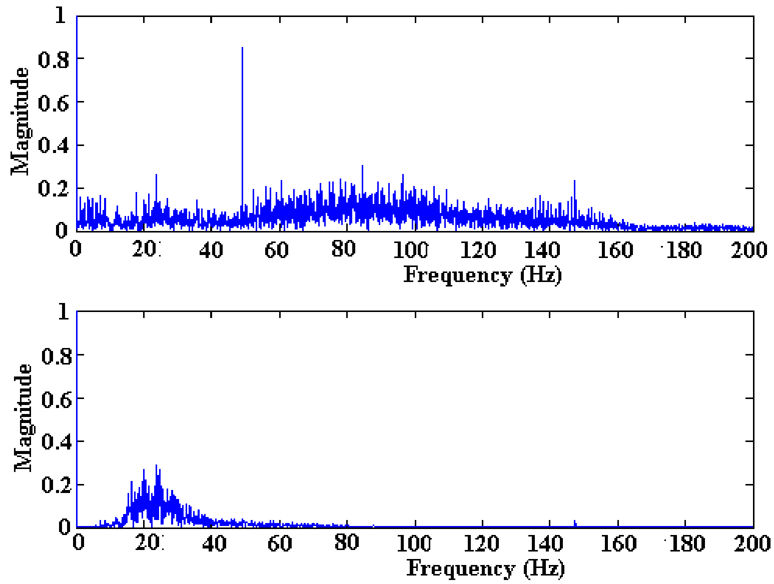

Fig 3.2 Magnitude spectra of PCG obtained using phonocardiograph sensors

3.3 Pulse pick up using piezoelectric transducer

The pulse waveform was also acquired by using a piezoelectric transducer ("Pamtrons"). It generates an electrical output when subjected to mechanical stresses due to the vibrations at the radial artery, and this electrical output is recorded. The transducer is kept in place over radial artery by closing the Velcro strap firmly around the wrist. Positioning is adjusted in order to get the optimal signal strength. The pulse waveform was recorded on a DSO. The amplitude of obtained pulse waveform is generally in the range of 400 mV-500 mV. Record with DSO has record length of 2000 samples. Fig 3.3 shows pulse waveform obtained by using Ts and piezoelectric transducer respectively. Magnitude spectra of the same are shown in Fig 3.4.

(a) Pulse using Ts

Voltage range: ± 900 mV

(b) Pulse using piezoelectric transducer

Voltage range: ± 400 mV

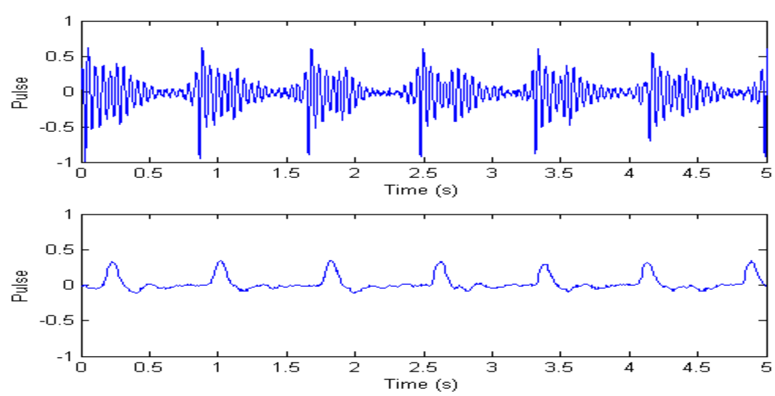

Fig 3.3 Pulse recorded using phonocardiograph sensor and piezoelectric transducer

(**a**) Spectrum: Pulse recorded using Ts

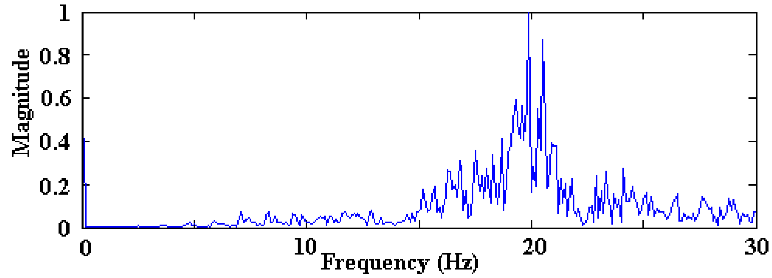

(**b**) Spectrum: Pulse recorded using piezoelectric transducer

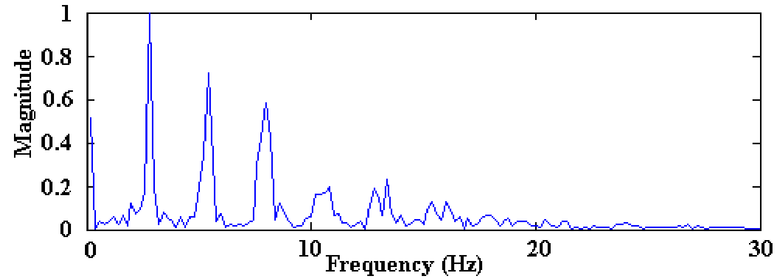

Fig 3.4 Magnitude spectra of pulse waveforms obtained using phonocardiograph sensor and piezoelectric transducer

Chapter 4
Signal enhancement

The signal obtained by using phonocardiograph is corrupted by noise, environmental sounds as well as the vibrations from various smaller blood vessels. This chapter outlines the noise reduction techniques for obtaining clean pulse waveform. Bandpass filtering did not show significant enhancement of pulse signal. Further it was decided to make use of spectral subtraction algorithm for enhancement of noisy pulse waveform and PCG. This algorithm is used for enhancement of noisy speech [19]. The algorithm takes a single input, which has two steps of operation, namely the noise estimation step and noise subtraction from the noisy signal, resulting in better quality output. For this purpose, estimate of noise spectrum can be obtained using noise recording from a nearby site or by using a quantile based spectral estimate of noise from the noisy pulse waveform itself.

4.1 Noise reduction by bandpass filter

For noise reduction, bandpass filtering was used. The bandpass filter was a FIR 256 coefficients digital filter having lower and upper cut-off frequencies 20 Hz and 200 Hz respectively. Fig 4.1 shows the magnitude response of bandpass filter. It has linear phase response. Fig 4.2 show PCG and pulse waveform, recorded by using the two phonocardiograph sensors and the band pass filtered versions.

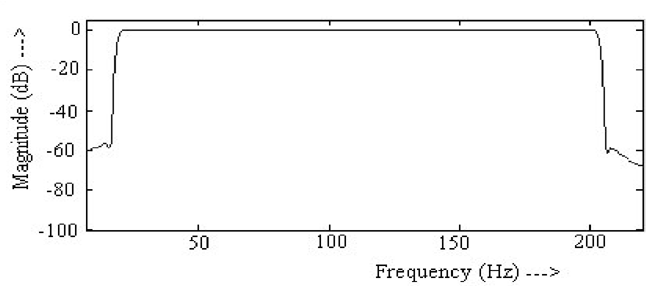

Fig 4.1 Magnitude response of bandpass filter

(a) PCG, acquired using Tm

(b) Bandpass filtered PCG

(c) Pulse waveform, acquired using Tm

(d) Bandpass filtered pulse waveform

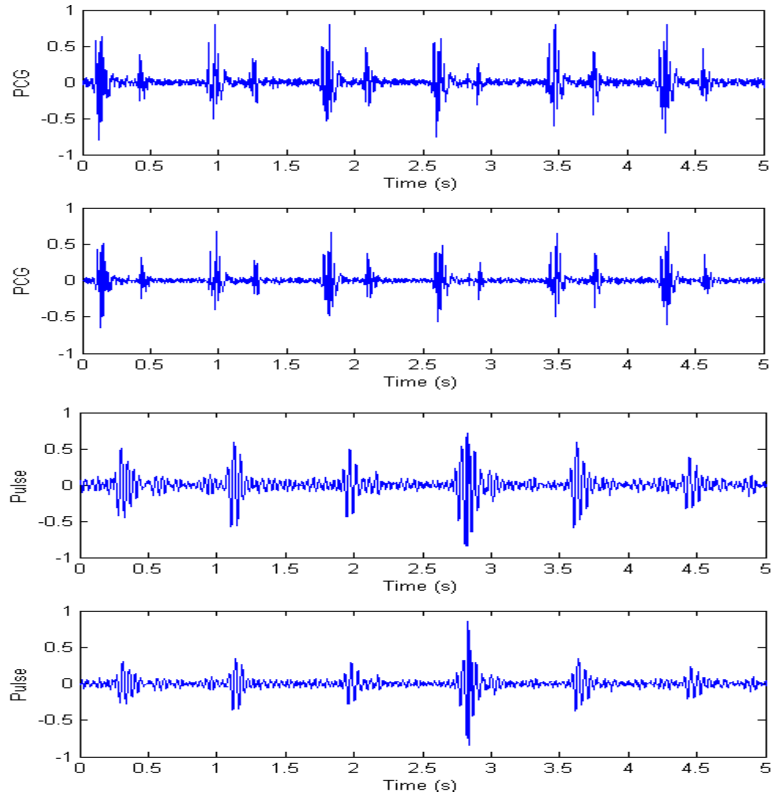

Fig 4.2 PCG and pulse waveform, recorded by PCG transducer

4.2 Cross-correlation after center clipping

Since the pulse waveform was corrupted with noise, center clipping [20] was done on band pass filtered pulse waveform, to enhance the contribution by peaks to the cross-correlated signal. Center clipping removes a certain fraction of the waveform. Let V_{max} be the maximum amplitude of the signal and V_{th} be the clipping level. Therefore, the output from the center clipper is

$$y(t) = x(t) \qquad \text{for } |x(t)| > V_{th}$$

$$0 \qquad \text{for } |x(t)| <= V_{th}$$

Hence for pulse signal below the clipping level, the output is zero, and for pulse signal above the clipping level, the output is equal to the actual recorded signal minus the clipping level.

Fig 4.3 show the PCG, pulse waveform and their processed versions. The band pass filter used is FIR type with lower and upper cut-off frequencies 20 Hz and 200 Hz.

As the PCG is relatively strong and noise free, center clipping is not needed for this signal. The pulse waveform recorded by using Ts is as shown in part c of Fig 4.3 and the processed pulse waveforms are as shown in part d, part e of Fig 4.3. Pulse signal is band pass filtered prior to center clipping. The threshold selected for clipping level is around 20% of maximum peak occurring in preprocessed pulse signal.

(a) PCG

(b) Bandpass filtered PCG

(c) Pulse waveform

(d) Bandpass filtered pulse waveform

(e) Bandpass filtered and center clipped pulse waveform

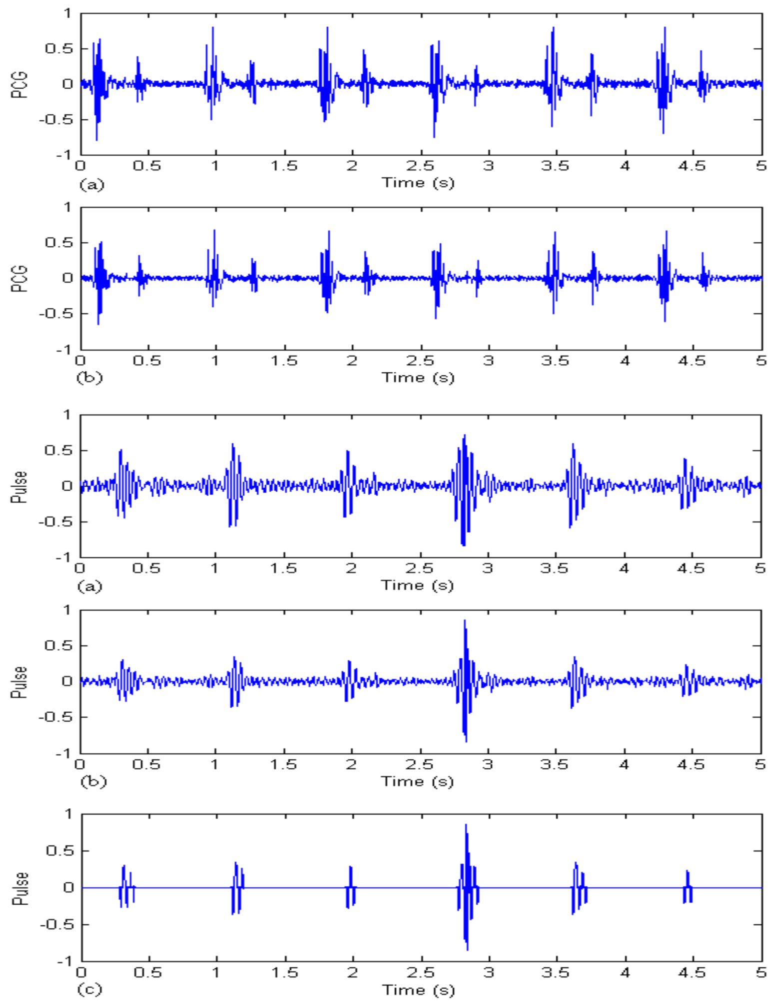

Fig 4.3 Processed (bandpass filtered, center clipped) PCG and pulse waveform

Fig 4.4 shows the cross-correlation between the unprocessed PCG and processed pulse waveforms, and center clipped pulse. For BPF waveform, the cross-correlation signal around the peaks is partly reduced. For center clipped waveform, it has almost disappeared. This indicates the peaks are enhanced in cross-correlation signal after center clipping. In order to observe the effect of band pass filtering of PCG on cross-correlation signal, the BP filtered PCG was cross-correlated with BPF pulse and BPF center clipped pulse and results are shown in Fig 4.5. We see that the peaks are enhanced in cross-correlation with BPF center clipped pulse. However, bandpass filtering of PCG is less effective in enhancing the peaks in cross-correlation signal, indicated by comparing Fig 4.4 with Fig 4.5. Zoomed versions of cross-correlation between PCG and processed pulse are shown in Fig 4.6. Maximum peak of the correlation occurs at 18.1 ms, as shown in part a of Fig 4.6, indicating time delay between PCG and pulse waveform. In parts b and c of Fig 4.6, delay between PCG and BPF pulse, between PCG and BPF, center clipped pulse respectively occur at 19.2 ms. Parts d, e of Fig 4.6, indicate delay between BPF PCG and BPF pulse, between BPF PCG and BPF, center clipped pulse as 18 ms.

(a) Cross-correlation with pulse (waveform of Fig 4.3a)

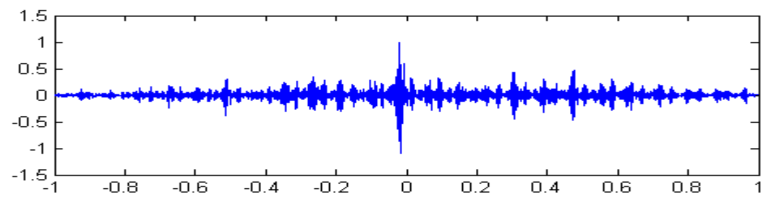

(b) Cross-correlation with BPF pulse (waveform of Fig 4.3b)

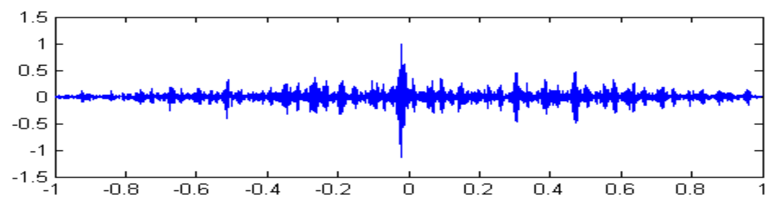

(c) Cross-correlation with BPF and center clipped pulse (waveform of Fig 4.3a)

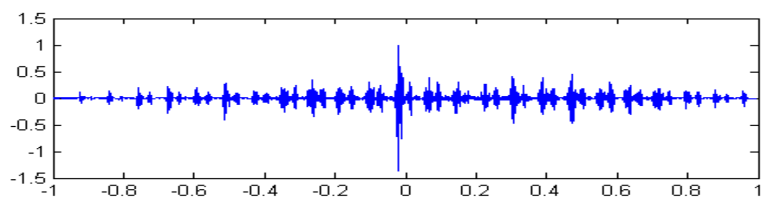

Fig 4.4 Cross-correlation between PCG and processed pulse waveform

(a) Cross-correlation with BPF pulse

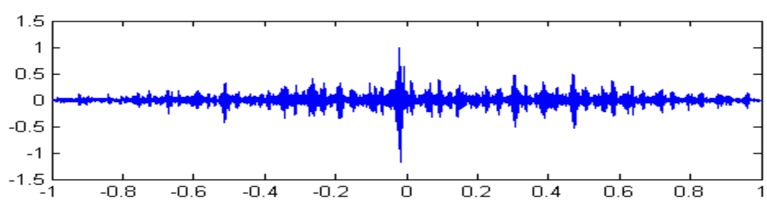

(b) Cross-correlation with BPF and center clipped pulse

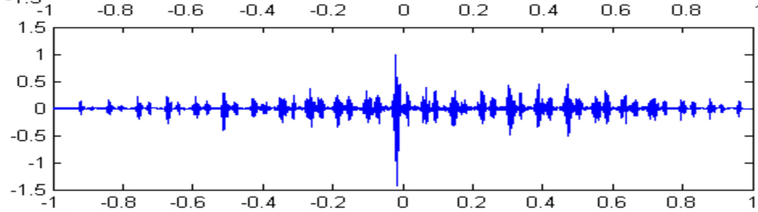

Fig 4.5 Cross-correlation between bandpass filtered PCG and processed pulse waveform (delay in s)

(a) Between PCG and pulse

(b) Between PCG and BPF pulse

(c) Between PCG and BPF, center clipped pulse

(d) Between BPF PCG and BPF pulse

(e) Between BPF PCG and BPF, center clipped pulse

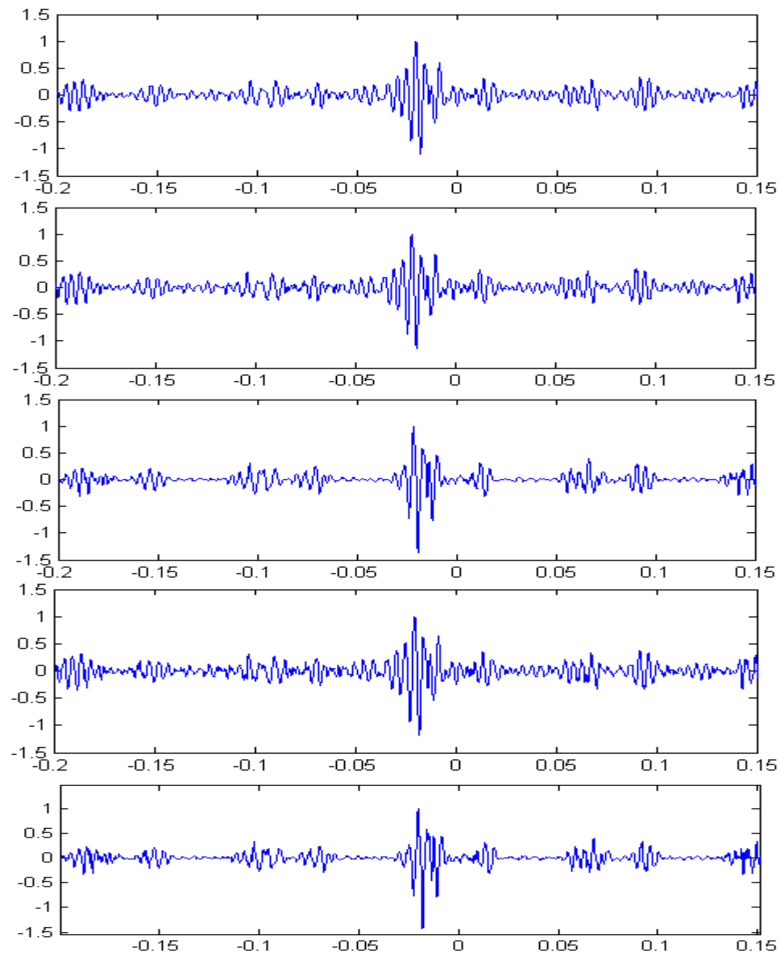

Fig 4.6 Zoomed version of cross-correlation waveform between PCG and processed pulse (delay in s)

However, both the methods did not show significant improvement on the pulse waveform. Hence it was decided to use the spectral subtraction algorithm, which is used for enhancing noisy speech signal.

4.3 Spectral subtraction

The basic assumption in spectral subtraction method [19][21][22], developed for enhancement of speech corrupted by noise, is that the clean signal and the noise are uncorrelated, and therefore the power spectrum of noisy signal equals the sum of magnitude spectrum of noise and clean signal. Let $x(n)$ be the windowed noisy signal consisting of the clean signal $s(n)$ and the additive noise $l(n)$. Hence the signal becomes,

$$x(n) = s(n) + l(n) \tag{4.1}$$

Taking short-time Fourier transform on both sides, we get

$$X_n\left(e^{jw}\right) = S_n\left(e^{jw}\right) + L_n\left(e^{jw}\right) \tag{4.2}$$

Assuming $s(n)$ and $l(n)$ to be uncorrelated, we get

$$\left|X_n\left(e^{jw}\right)\right|^2 = \left|S_n\left(e^{jw}\right)\right|^2 + \left|L_n\left(e^{jw}\right)\right|^2 \tag{4.3}$$

The basic spectral subtraction algorithm works in two steps (i) noise spectrum is estimated and (ii) the estimated noise spectrum is subtracted from that of the noisy signal to get

$$\left|Y_n\left(e^{jw}\right)\right|^2 = \left|X_n\left(e^{jw}\right)\right|^2 - \left|L_n\left(e^{jw}\right)\right|^2 \tag{4.4}$$

The resulting magnitude spectrum is then combined with the original phase spectrum to resynthesize the "cleaned" signal. Using FFT for implementation, the steps can be written as

$$\left|Y_n(k)\right|^2 = \left|X_n(k)\right|^2 - \left|L(k)\right|^2 \tag{4.5}$$

$$y_n(m) = IFFT\left[\left|Y_n(k)\right| e^{j\angle X_n(k)}\right] \tag{4.6}$$

When the estimate of the noise spectrum is subtracted from the actual noise spectrum, all the spectral peaks are shifted down while the points lower than the estimate are set to zero. Hence, noise spectrum obtained after subtraction has peaks. The wider peaks give broadband noise and the narrower peaks give the musical noise. Thus the spectral subtraction method is modified for minimizing this noise [19].

$$\left|Y_n(k)\right|^2 = \left|X_n(k)\right|^2 - \alpha\left|L(k)\right|^2$$

and

$$\left|Y'_n(k)\right|^2 = \begin{cases} \left|Y_n(k)\right|^2 & \text{if } \left|Y_n(k)\right|^2 > \beta\left|L(k)\right|^2 \\ \beta\left|L(k)\right|^2 & \text{otherwise} \end{cases} \tag{4.7}$$

where α is the subtraction factor and β is the spectral floor factor.

A block diagram of the modified spectral subtraction algorithm is as shown in Fig 4.7.

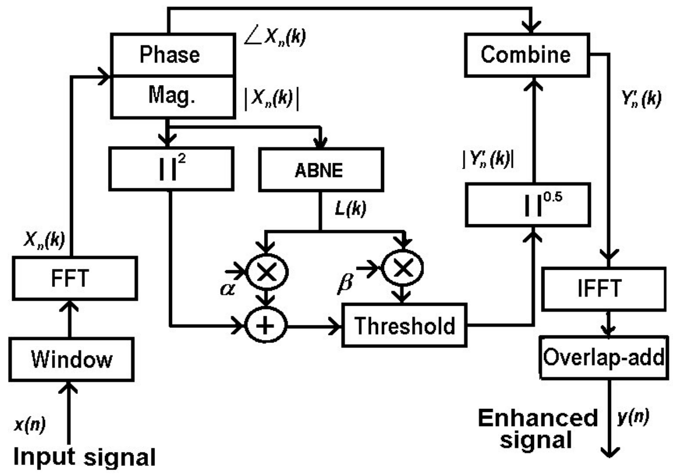

Fig 4.7 Block diagram of modified spectral subtraction algorithm [19]

With $\alpha > 1$, the noise will be over subtracted from the noisy signal. However over subtraction increases signal distortion. This is taken care by the spectral floor factor β. The spectral components of $|Y'_n(k)|^2$ are prevented from going below $\beta|L(k)|^2$. The implementation via FFT requires technique like overlap-and-add in order to prevent discontinuities at frame boundaries [18][21].

4.4 Noise estimation by averaging

For simultaneous acquisition of PCG and noise, sensor Tm was kept on the position of heart on the chest and sensor Ts was kept over chest only, but away from the position of the heart. Hence PCG and noise on the chest were recorded simultaneously. Similarly, for pulse waveform, sensor Ts was kept over radial artery on the wrist and sensor Tm was kept on the same hand but away from the radial artery. A sampling rate of 1.1, 025 k sa/s (11.025 k sa/s, followed by 10:1 decimation) was used. The averaged noise spectrum was computed over different averaging durations, using 1.6 s window with 50% overlap. This average spectrum is used for spectral subtraction.

4.4.1 Effect of averaging duration, selected for noise estimation over PCG and pulse waveform

In spectral subtraction algorithm, the averaging duration is the time interval over which recorded noise signal is windowed and averaged for estimating the noise. Hence by selecting averaging duration as T = 2, 4, 16 s, the signals were analyzed for different values of α.

Effect of averaging duration of noise over PCG

In order to analyze the effect of averaging duration used for noise estimation, the spectral subtraction algorithm is used on PCG, by estimating noise over 2, 4 and 16 s. The unprocessed PCG and noise are shown in Fig 4.8. Average and standard deviation (S.D.) of the magnitude spectra of noise were obtained for different durations. It was observed that S.D. decreased with the averaging duration. Fig 4.9 shows the S.D. for T = 2 s and 16 s, and we see that for the larger duration it is much less for almost all frequency samples. The noise spectra averaged for T = 2, 4 and 16 s were used for spectral subtraction and the processed PCG output is shown in Fig 4.10 and 4.11 for α = 1 and 5 respectively. We see that oversubtraction occurs on the PCG processed with noise estimated over lesser averaging duration, and a more uniformly enhanced PCG is obtained for the larger averaging duration.

Effect of averaging duration of noise over pulse waveform

The spectral subtraction algorithm was also used on pulse waveform by estimating noise over T = 2, 4 and 16 s. Fig 4.12 shows unprocessed pulse waveform and noise over a 5 s duration. Average and standard deviation of the magnitude spectra of noise were obtained for different durations. It was observed that S.D. decreased with the averaging duration. Fig 4.13 shows the S.D. for T = 2 s and 16 s, and we see that the one for the larger duration is much less for almost all frequency samples. The noise spectra averaged for T = 2, 4 and 16 s were used for spectral subtraction and the processed pulse output is shown in Fig 4.14 and 4.15 for α = 1 and 5 respectively. We see that oversubtraction occurs on the pulse waveform processed with noise estimated over lesser averaging duration, and a more uniformly enhanced pulse waveform is obtained for the larger averaging duration.

(a) Unprocessed PCG

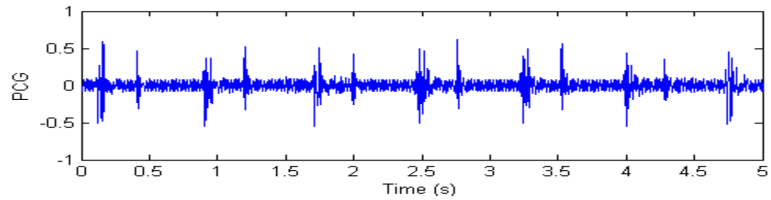

(b) Noise

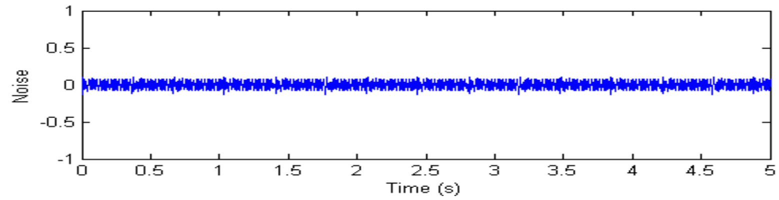

Fig 4.8 PCG and noise recorded simultaneously

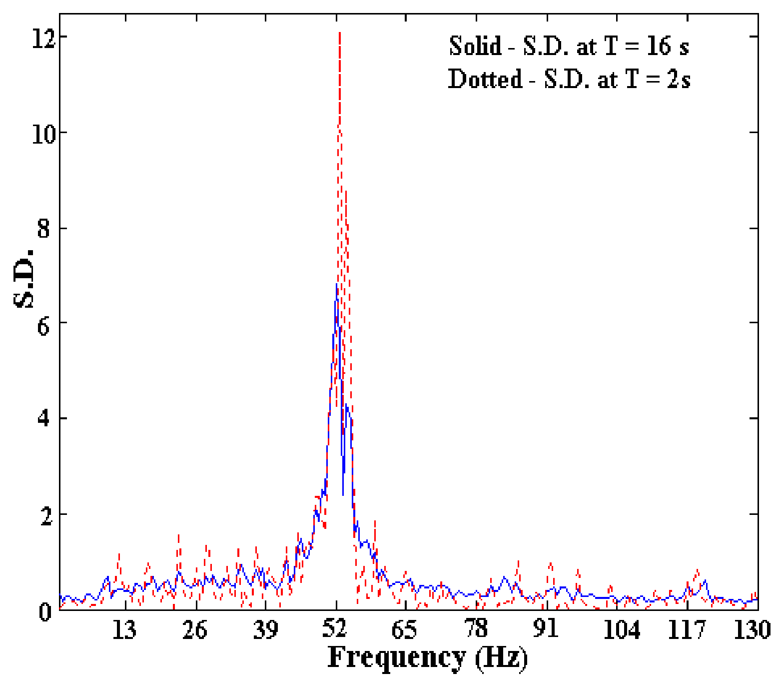

Fig 4.9 Plot of S.D. of noise estimate vs. frequency used for PCG

(a) $T = 2$ s

(b) $T = 4$ s

(c) $T = 16$ s

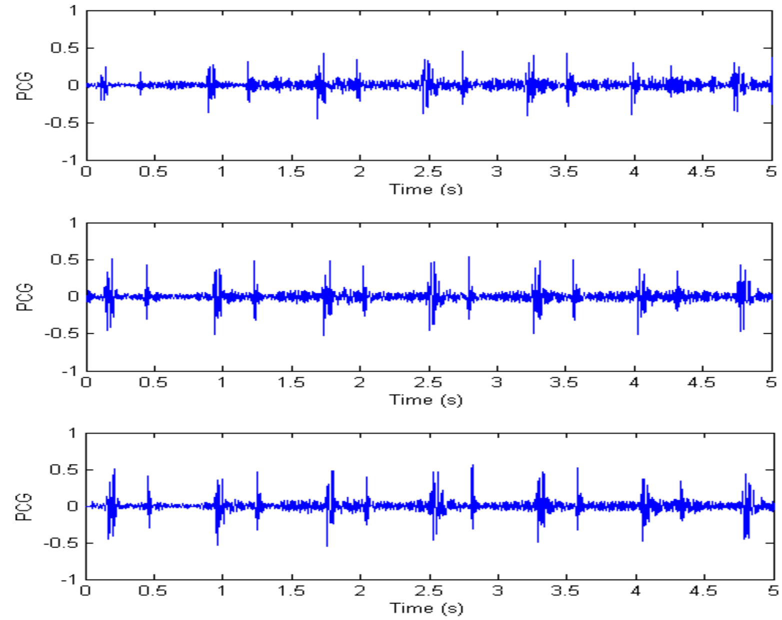

Fig 4.10 Processed PCG for $\alpha = 1$

(a) $T = 2$ s

(b) $T = 4$ s

(c) $T = 16$ s

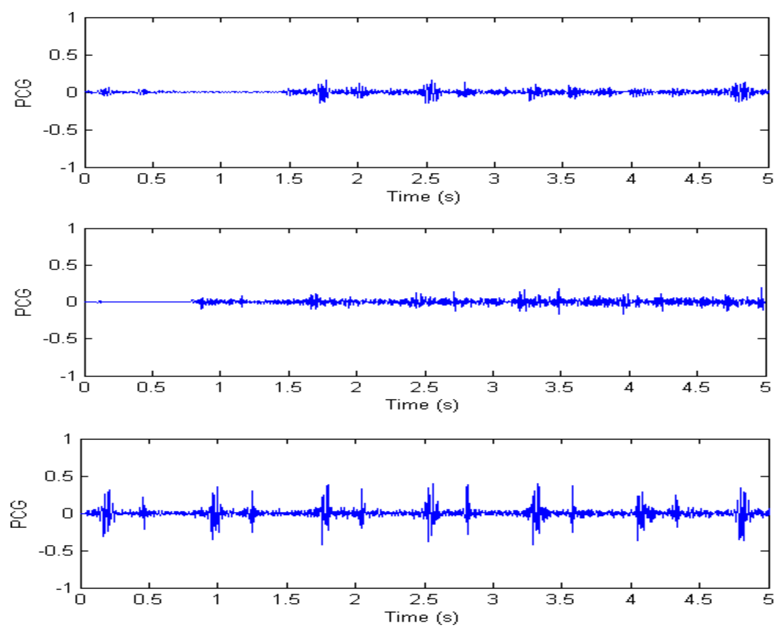

Fig 4.11 Processed PCG for $\alpha = 5$

(a) Unprocessed pulse waveform

(b) Noise

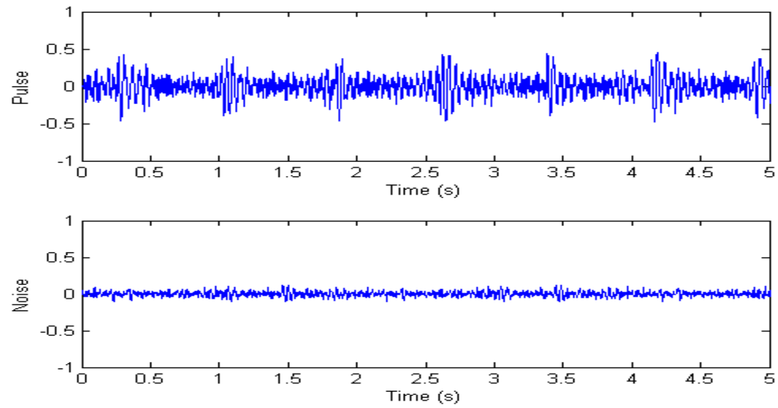

Fig 4.12 Pulse waveform and noise recorded simultaneously

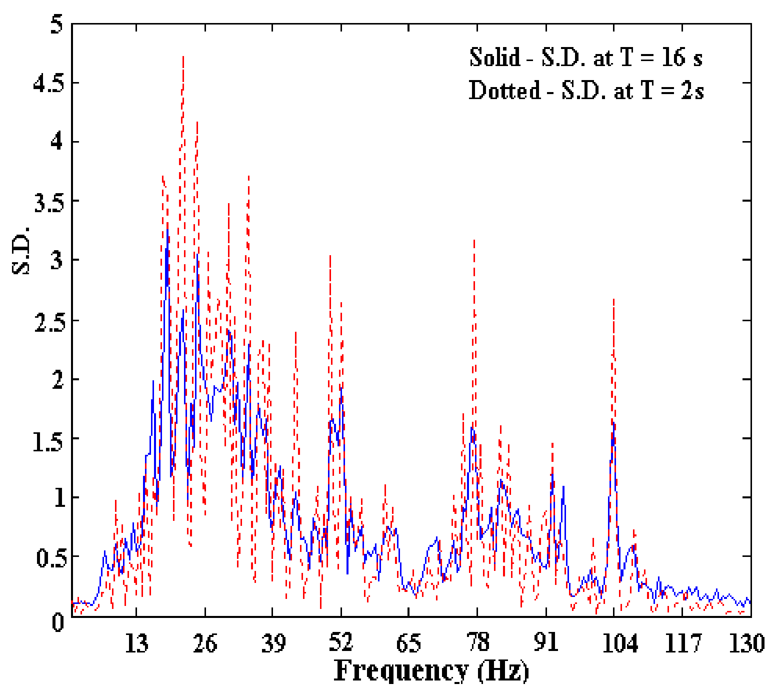

Fig 4.13 Plot of S.D. of noise estimate vs. frequency used for pulse signal

(a) $T = 2$ s

(b) $T = 4$ s

(c) $T = 16$ s

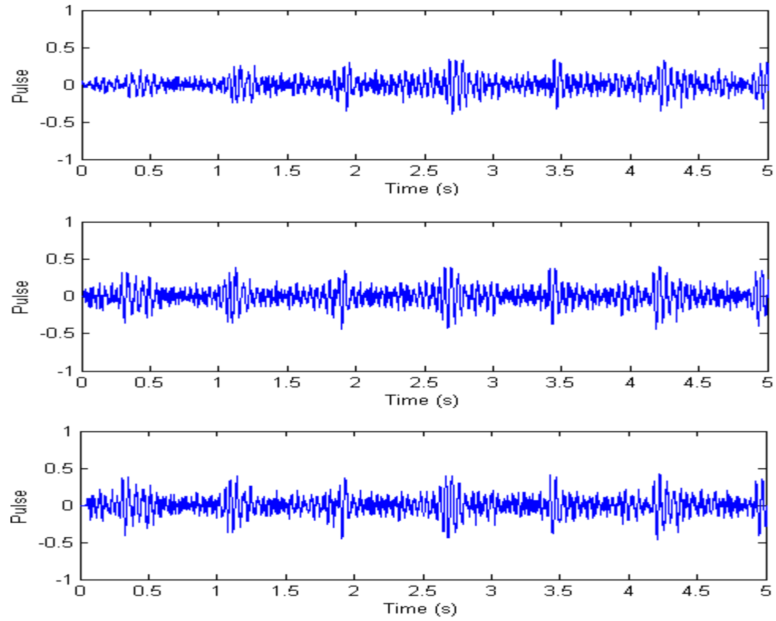

Fig 4.14 Processed pulse waveform for $\alpha = 1$

(a) $T = 2$ s

(b) $T = 4$ s

(c) $T = 16$ s

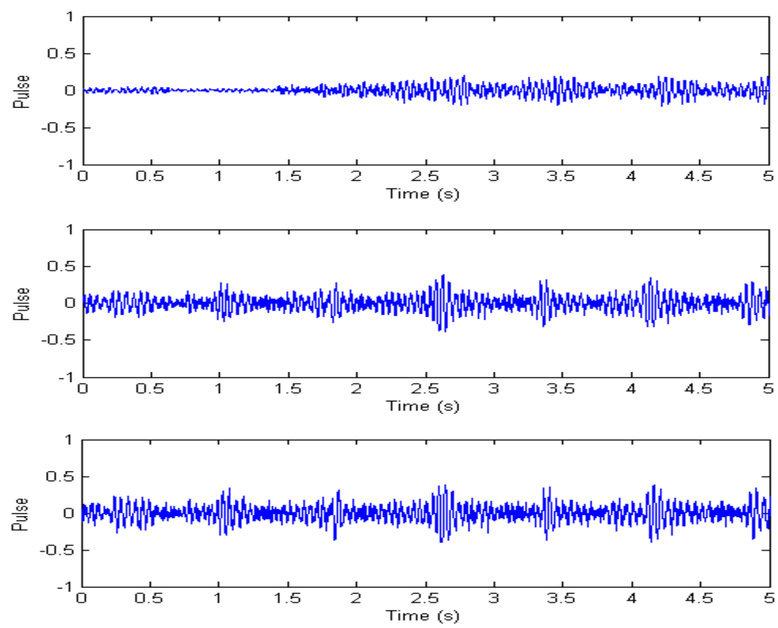

Fig 4.15 Processed pulse waveform for $\alpha = 5$

4.4.2 Effect of noise site on PCG

For analyzing the effect of noise site on enhancement of PCG, noise was acquired from two sites, i.e. noise acquired by keeping phonocardiographic instrument on the chest but away from the heart position and the noise acquired by keeping phonocardiographic instrument on the hand but away from the radial artery. Fig 4.16 shows the PCG, before using spectral subtraction method with noise acquired from the hand and chest. By keeping T = 16 s and α = 1, PCG is processed. From Fig 4.17, it is observed the noise recorded on the chest results in better enhancement of PCG as compared to that with noise recorded from the hand. Hence we decided to use noise estimate from recording sites close to signal site. Further, if the noise can be estimated from the signal site itself, it is likely to give superior enhancement.

(a) Unprocessed PCG

(b) Noise recorded from hand

(c) Noise recorded from chest

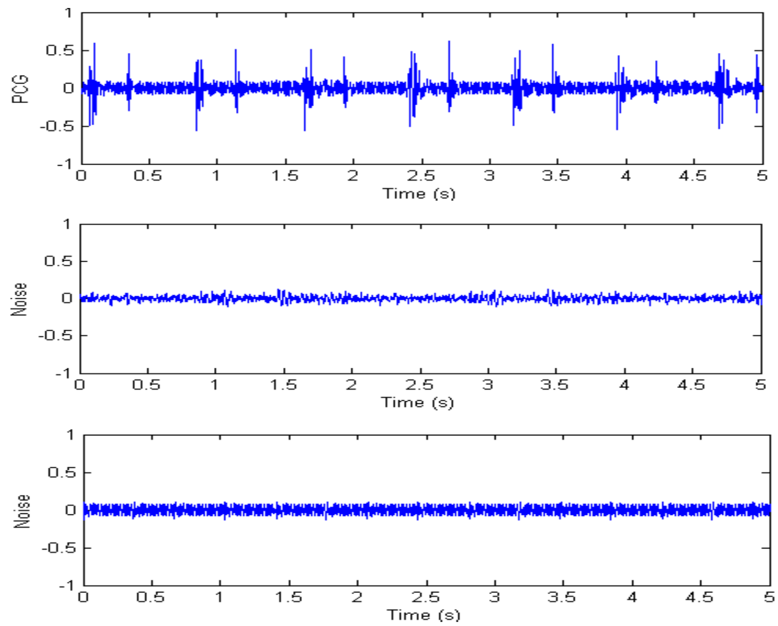

Fig 4.16 Unprocessed PCG and noise

(a) Processed PCG with noise recorded from hand

(b) Processed PCG with noise recorded from chest

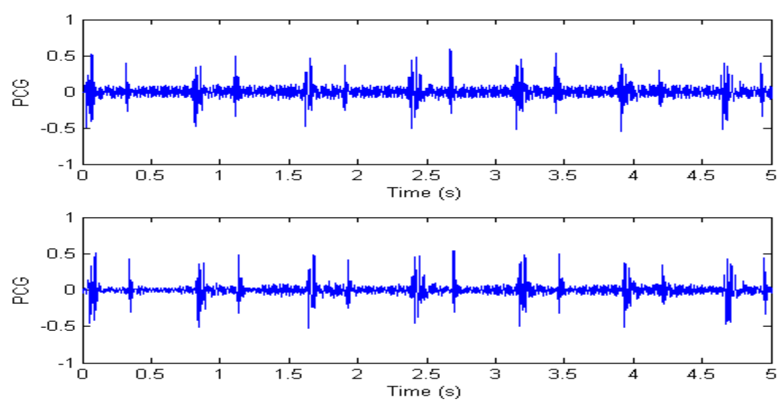

Fig 4.17 Processed PCG with noise recorded from hand and chest at $\alpha = 1$

4.4.3 Effect of spectral subtraction on cross-correlation waveform

The effect of noise is observed by cross-correlating the unprocessed PCG and unprocessed pulse waveform. Also the PCG after using spectral subtraction method is cross-correlated with processed pulse waveform and effect of spectral subtraction method is observed. Fig 4.18 shows PCG and enhanced PCG after using spectral subtraction. Unprocessed pulse and processed pulse are shown in Fig 4.19. Fig 4.20 shows cross-correlation between unprocessed PCG and unprocessed pulse waveform, between processed PCG and processed pulse respectively. Zoomed versions of cross-correlation waveforms are shown in Fig 4.21. In Fig 4.20 and 4.21, it is observed that the cross-correlation signal away from the peak is reduced after using the spectral subtraction, indicating enhancement of peaks in cross-correlation signal.

(a) Unprocessed PCG

(b) Processed PCG

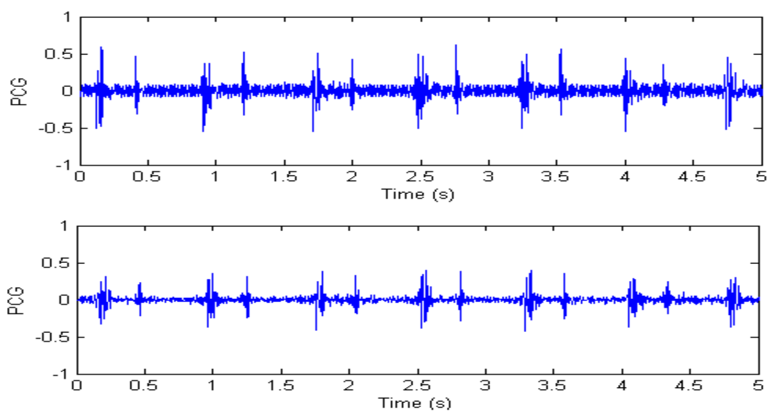

Fig 4.18 PCG (unprocessed and processed)

(a) Unprocessed pulse

(b) Processed pulse

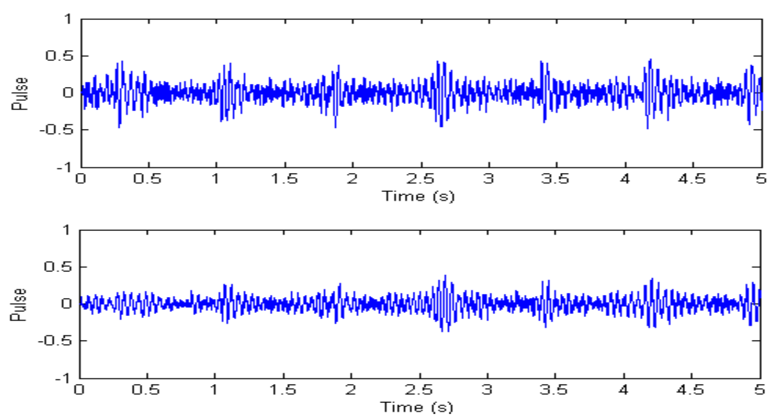

Fig 4.19 Pulse waveform (unprocessed and processed)

(a) Before using spectral subtraction

(b) After using spectral subtraction

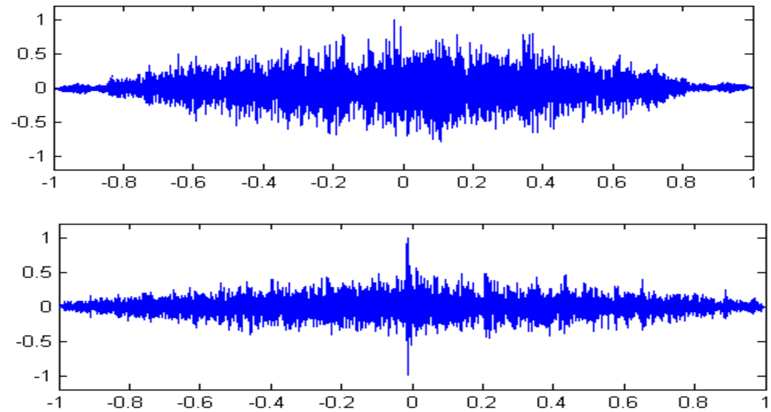

Fig 4.20 Cross-correlation waveform between PCG and pulse signal

(a) Before using spectral subtraction

(b) After using spectral subtraction

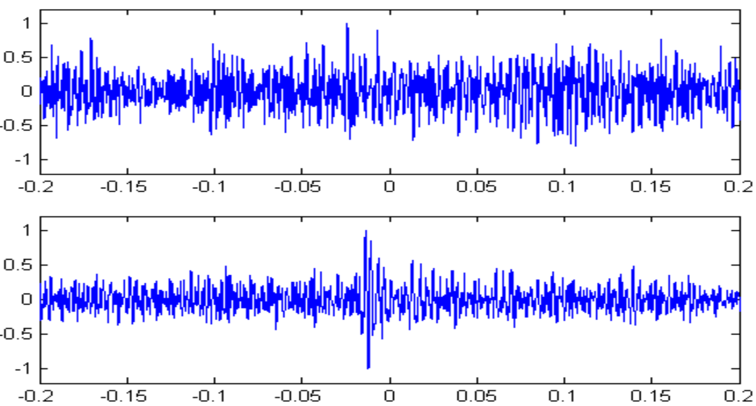

Fig 4.21 Zoomed version of Cross-correlation waveform between PCG and pulse signal

4.5 Quantile-based noise estimation (QBNE) technique

In the earlier method, the noise spectrum is taken to be constant over the entire duration of the signal to be enhanced. An updated estimate of noise spectrum can be obtained by use of quantile-based noise estimation technique [23][24]. It is based on the assumption that the frequency bins in the signal spectrum tend not to be permanently occupied by the signal. The noisy pulse signal is analyzed on a frame-by-frame basis, to obtain an array of power spectral values for each frequency sample, for a certain number of frames. Then the magnitude-squared values in this array are sorted for obtaining a particular quantile value. The power spectrum of noisy pulse at different values is compared with the mean power spectrum of noise recorded from the nearby site for obtaining the quantiles in frequency bands for matching the two spectra.

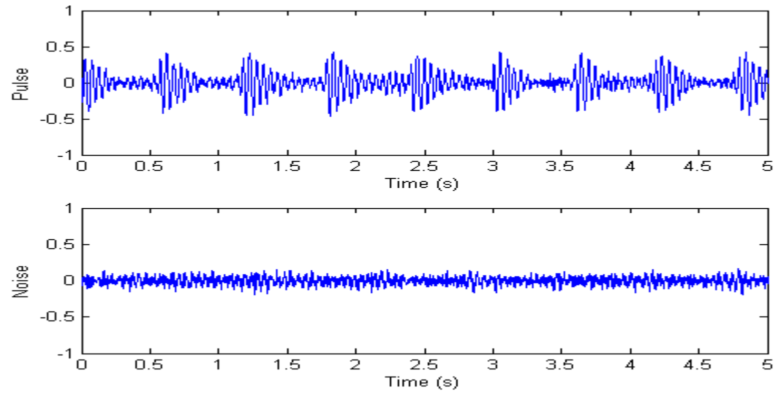

Fig 4.22 Noisy pulse waveform and noise

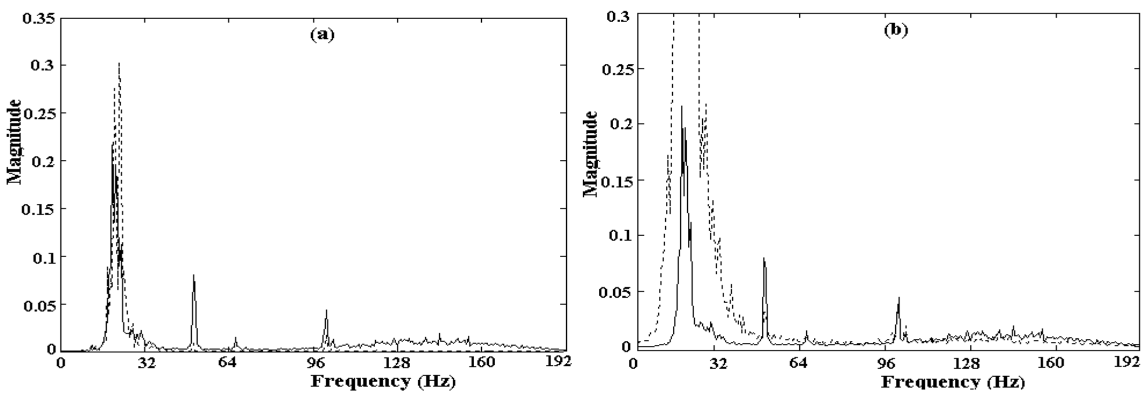

Fig 4.23 Averaged noise spectrum and QBNE spectrum for **(a)** 5 percentile and **(b)** 70 percentile. Plot with solid line shows the average power spectrum of noise and plot with dotted line shows the quantile-derived spectrum of noisy pulse.

For QBNE, the radial arterial pulse and noise was recorded at several sites on the same hand by using Ts. Fig 4.22 shows the pulse and noise recorded on the same hand. Further the averaged spectrum of noise from the nearby site was compared with the spectrum of noisy pulse at different quantile values to obtain set of quantile values for giving close match. Fig 4.23 shows the averaged spectrum of noise and two quantile-based estimates. It is observed that a good match could be obtained for 5 percentile for frequencies lesser than 32 Hz and 70 percentile for higher frequencies. Further the spectral subtraction was carried out on noisy pulse waveform with $\beta = 0.001$ and varying α over 0.5 to 5. Fig 4.24 shows an example of one such enhanced pulse waveform using QBNE spectrum.

(a) Unprocessed pulse waveform

(b) Enhanced pulse waveform

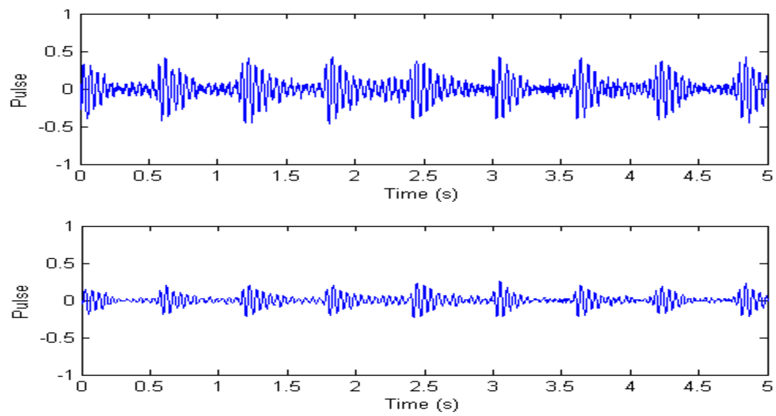

Fig 4.24 Enhanced pulse waveform by using noise estimation from noisy pulse using QBNE, using $\alpha = 2$.

4.5.1 Effect of noise estimate and oversubtraction

It is seen that the value of α and the type of noise estimate both have significant effect on noise reduction as well as over-subtraction. In order to observe this, the spectral subtraction was carried out on noisy pulse waveform using β = 0.001 and varying α over 0.5 to 5. Then the results of enhanced pulse waveform using noise estimate by averaging and quantile-based spectra were compared. Fig 4.25 shows the unprocessed pulse waveform. Fig 4.26 shows processed pulse waveforms using noise estimation by averaging and quantile-based spectra at α = 0.5, α = 2 and α = 5 respectively. From Fig 4.26, it is seen that the lower value of α does not result in good noise subtraction, while larger values of α results in oversubtraction.

In order to establish the effectiveness of the noise subtraction without signal loss, we make use of the observation that the pulse signal has a strong peak and very low value after the peak. A decrease in the peak can be taken as an indication of signal loss. While a decrease in overall signal without decrease in the peak can be taken as reduction in the background noise. For this purpose, the RMS value of the overall signal and the RMS value of signal samples in the vicinity of the pulse peaks were calculated. Table 4.1 shows the values of pulse peak and pulse signal for different values of α. Fig 4.27 shows the plot of these RMS values as a function of α for the two types of the noise estimates. It is seen that for average-based noise estimate (ABNE), both the RMS values decrease with increasing α. For QBNE spectrum, the noise estimation is much more effective. For

α > 2, the peak RMS decreases without any further decrease in signal RMS. Hence we can say that we get the best signal enhancement by using QBNE spectrum for $\alpha \approx 2$.

Fig 4.25

Unprocessed pulse waveform

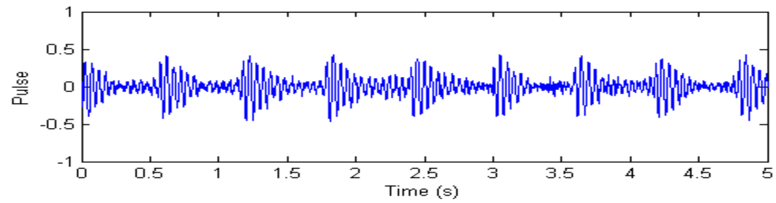

(a) Spectrum: ABNE

$\alpha = 0.5$

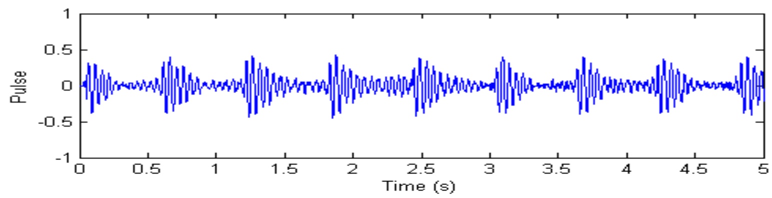

(b) Spectrum: QBNE

$\alpha = 0.5$

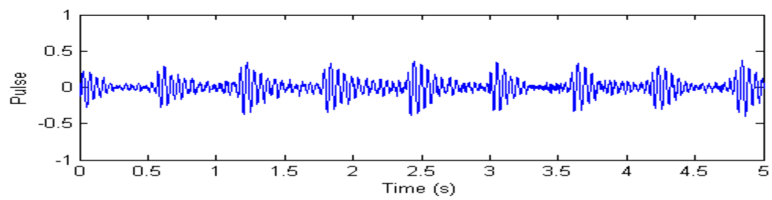

(c) Spectrum: ABNE

$\alpha = 2$

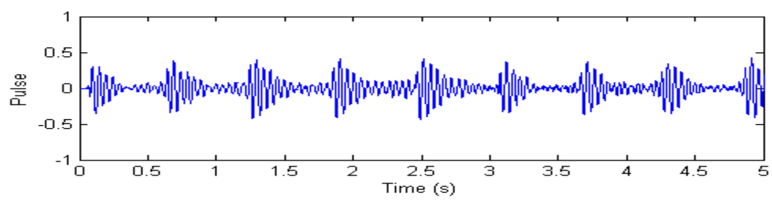

(d) Spectrum: QBNE

$\alpha = 2$

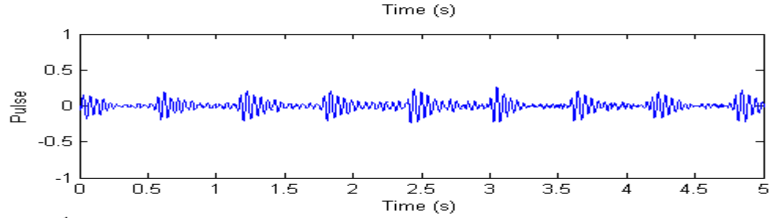

(e) Spectrum: ABNE

$\alpha = 5$

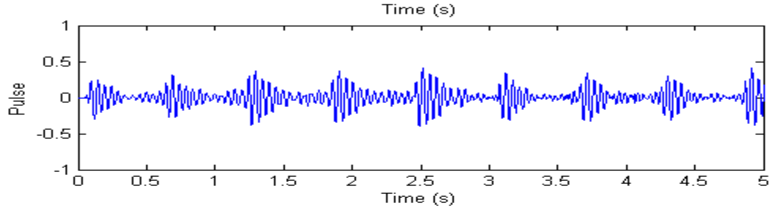

(f) Spectrum: QBNE

$\alpha = 5$

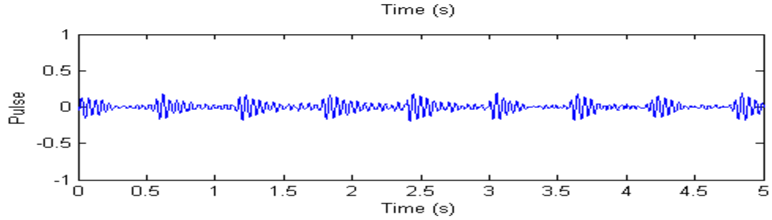

Fig 4.26 Processed pulse waveform with noise estimate using ABNE and QBNE spectra with α = 0.5, 2 and 5.

Table 4.1 Variation of pulse signal and pulse peak with respect to α for averaged noise estimation and QBNE method.

Noise estimation	α	Overall RMS	Peak RMS	Peak-to-overall ratio
ABNE	0.5	0.133	0.226	0.588
	1	0.131	0.225	1.718
	2	0.126	0.221	1.754
	3	0.122	0.219	1.795
	4	0.118	0.217	1.839
	5	0.115	0.215	1.870
QBNE	0.5	0.118	0.212	1.797
	1	0.097	0.210	2.165
	2	0.075	0.202	2.693
	3	0.067	0.198	2.955
	4	0.063	0.191	3.032
	5	0.063	0.184	2.921

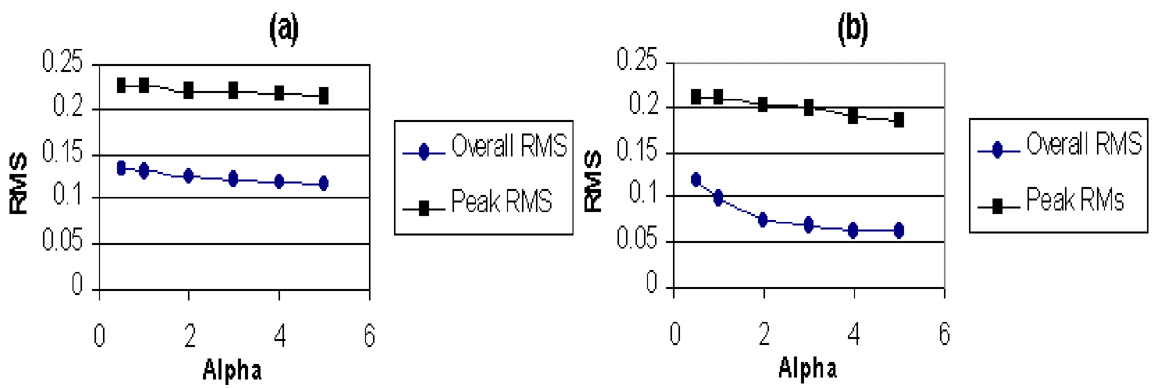

Fig 4.27 Effect of α on reduction of noise and peak **(a)** with averaged noise spectrum and **(b)** with QBNE for results in Table 4.1

4.5.2 Effect of spectral subtraction on cross-correlation waveform

The effect of spectral subtraction is observed by cross-correlating PCG with unprocessed pulse waveform. Also the PCG is cross-correlated with processed pulse waveforms with QBNE. Fig 4.28 shows PCG, unprocessed pulse and processed pulse waveforms. Fig 4.29 shows cross-correlation between PCG and unprocessed pulse waveform, between PCG and processed pulse waveforms respectively. Zoomed versions of cross-correlation waveforms are shown in Fig 4.30. In Fig 4.29 and 4.30, it is observed that the cross-correlation signal away from the peak is reduced after using the spectral subtraction, indicating enhancement of peaks in cross-correlation signal.

(a) Unprocessed PCG

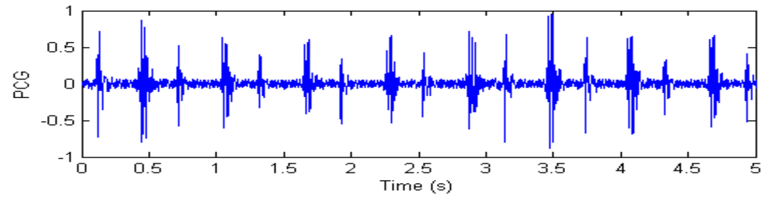

(b) Unprocessed pulse

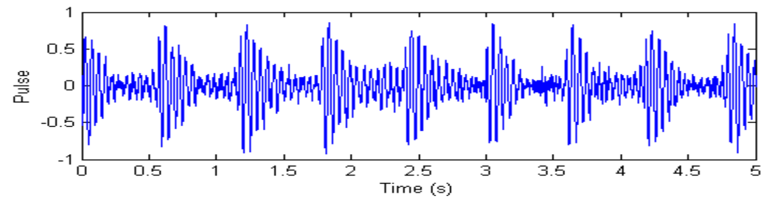

(c) Enhanced pulse, using QBNE

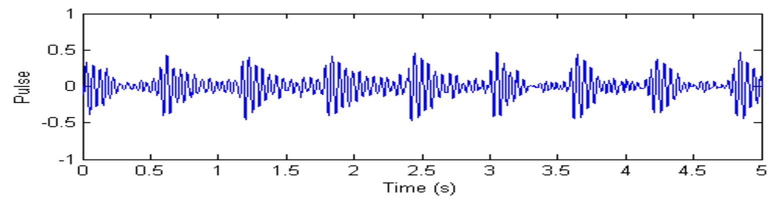

Fig 4.28 PCG and pulse waveform (unprocessed and processed)

(a) Before using spectral subtraction

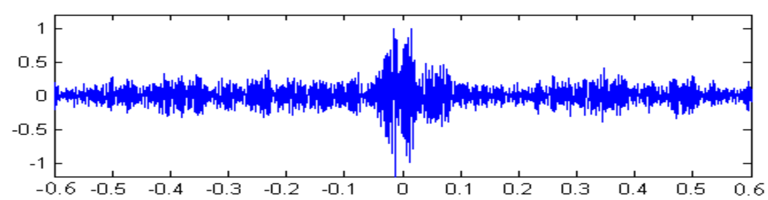

(b) After using spectral subtraction

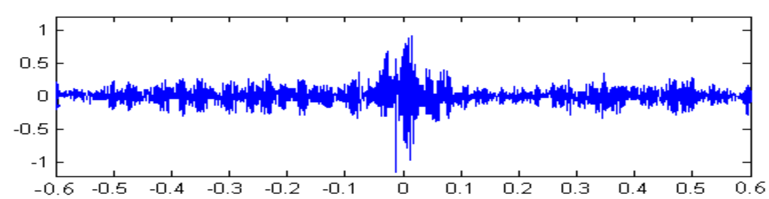

Fig 4.29 Cross-correlation waveform between PCG and pulse waveform

(a) Before using spectral subtraction

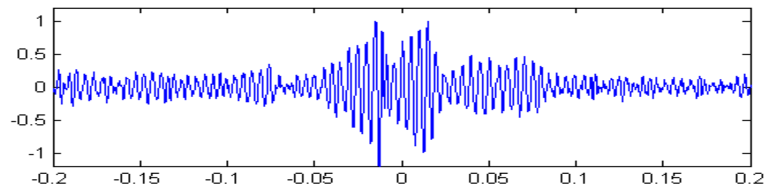

(b) After using spectral subtraction

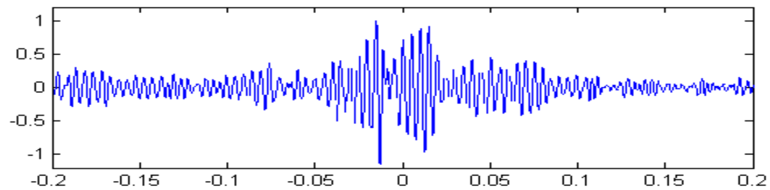

Fig 4.30 Zoomed version of cross-correlation waveform between PCG and pulse signal

4.6 Sample results

Pulse waveforms were recorded using Ts on two different subjects. Further, enhanced pulse waveforms are obtained by using noise estimate from nearby site and QBNE technique with α = 2. Fig 4.31 shows unprocessed PCG and pulse waveform recorded from S1_Ma, enhanced pulse waveforms by using noise estimate from nearby site and by using QBNE technique respectively. Magnitude spectra of unprocessed pulse, enhanced pulse with noise estimate from nearby site and QBNE technique respectively are shown in Fig 4.32. The effect of spectral subtraction on cross-correlation waveform is observed by cross-correlating PCG with unprocessed and processed pulse waveforms with noise estimated from nearby site and QBNE. Fig 4.33 shows cross-correlation between PCG and unprocessed pulse waveform, between PCG and processed pulse waveforms respectively. Zoomed versions of cross-correlation waveforms are shown in Fig 4.34. The noisy pulse waveform recorded from S2_Pr, enhanced pulse waveforms by using noise estimate from nearby site and QBNE technique are shown in Fig 4.35. Magnitude spectra of the same signals are as shown Fig 4.36. Fig 4.37 shows cross-correlation between PCG and unprocessed pulse waveform, between PCG and processed pulse waveforms respectively. Zoomed versions of cross-correlation waveforms are shown in Fig 4.38.

(a) Unprocessed PCG

(b) Unprocessed pulse waveform

(c) Enhanced pulse signal, using ABNE

(d) Enhanced pulse signal, using QBNE

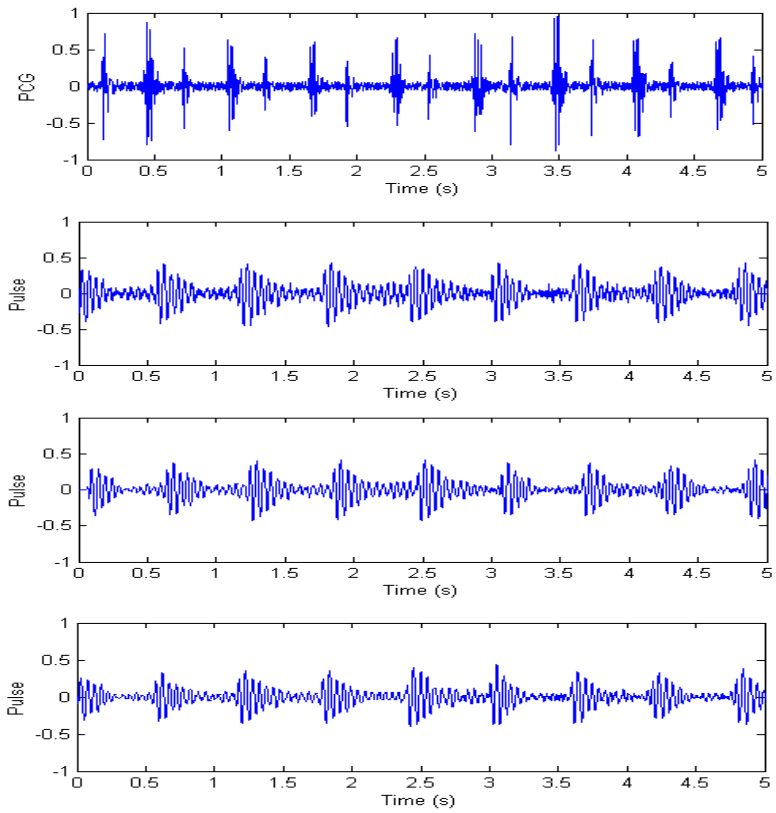

Fig 4.31 PCG and pulse waveforms recorded from subject S1_Ma (M, 30 years)

(a) Noisy pulse signal

(b) Pulse signal enhanced using ABNE

(c) Pulse signal enhanced using QBNE

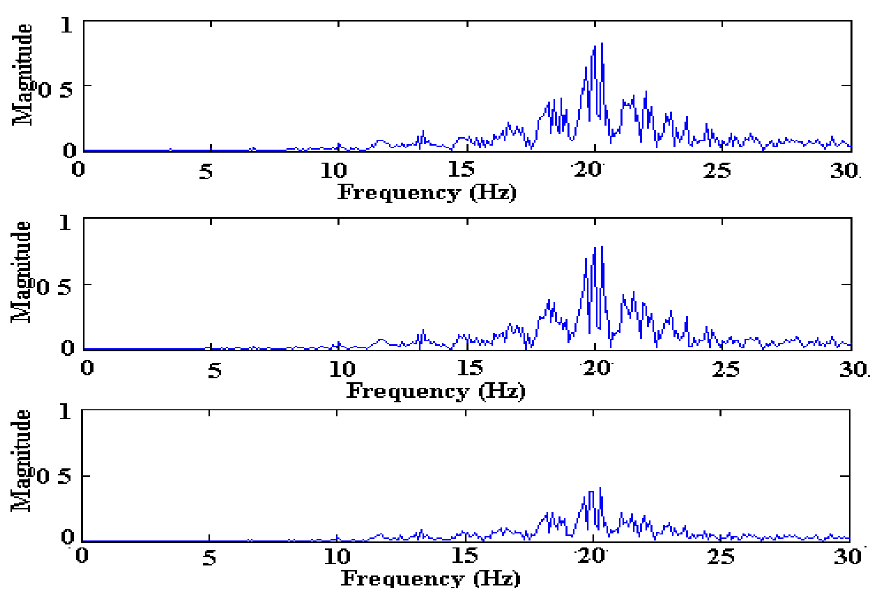

Fig 4.32 Magnitude spectra of pulse waveforms for subject S1_Ma

(a) Before using spectral subtraction

(b) After using spectral subtraction (ABNE)

(c) After using spectral subtraction (QBNE)

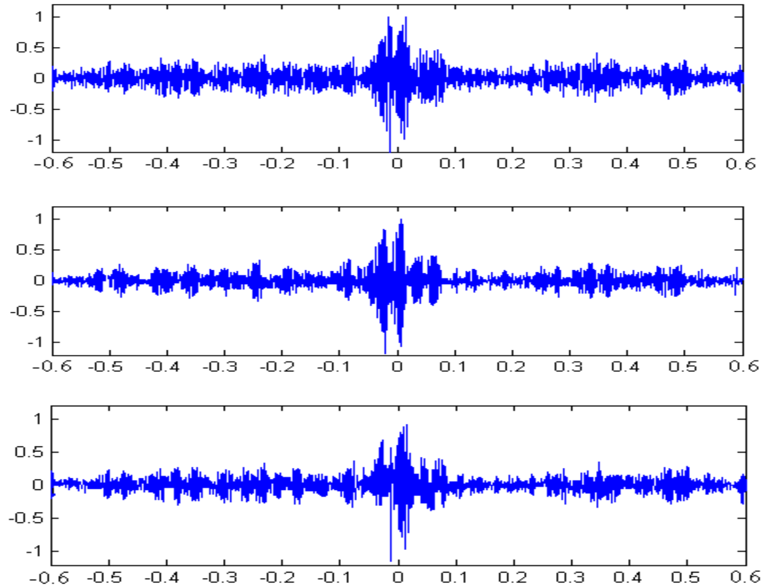

Fig 4.33 Cross-correlation waveform between PCG and pulse waveform for subject S1_Ma

(a) Before using spectral subtraction

(b) After using spectral subtraction (ABNE)

(c) After using spectral subtraction (QBNE)

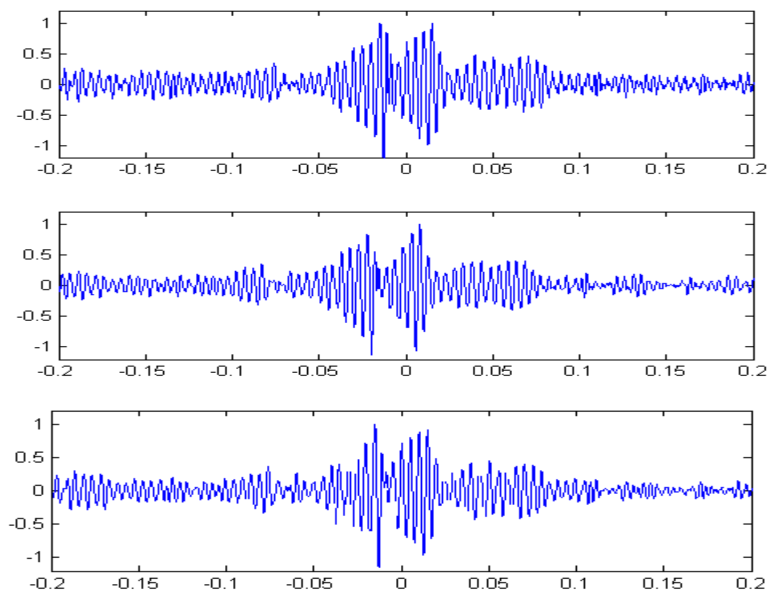

Fig 4.34 Zoomed version of cross-correlation waveform between PCG and pulse signal for subject S1_Ma

(a) Unprocessed PCG

(b) Unprocessed pulse waveform

(c) Enhanced pulse signal, using ABNE

(d) Enhanced pulse signal, using QBNE

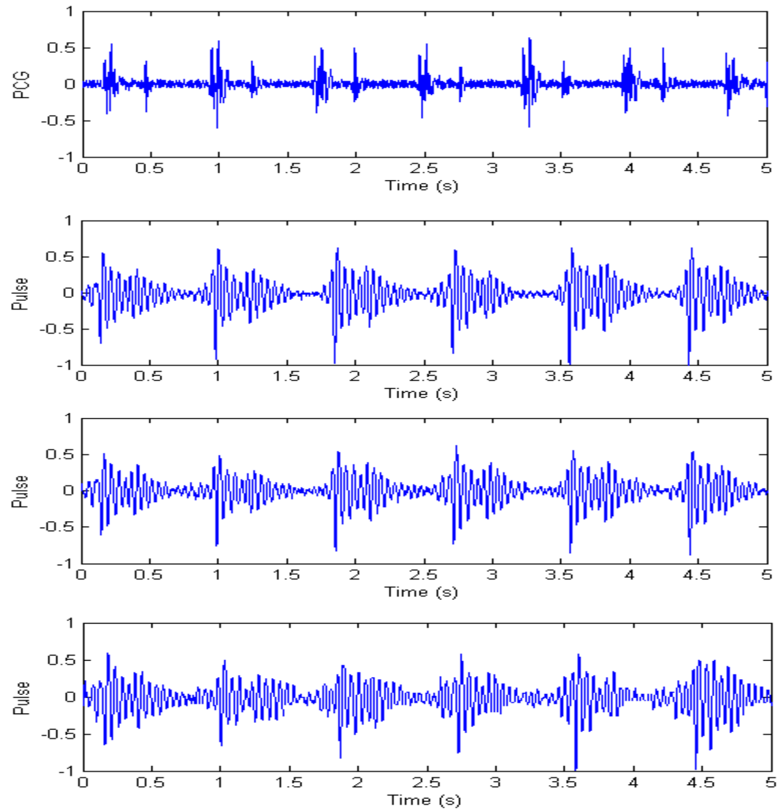

Fig 4.35 PCG and pulse waveforms recorded from subject S2_Pr (M, 38 years)

(a) Noisy pulse signal

(b) Pulse signal enhanced using ABNE

(c) Pulse signal enhanced using QBNE

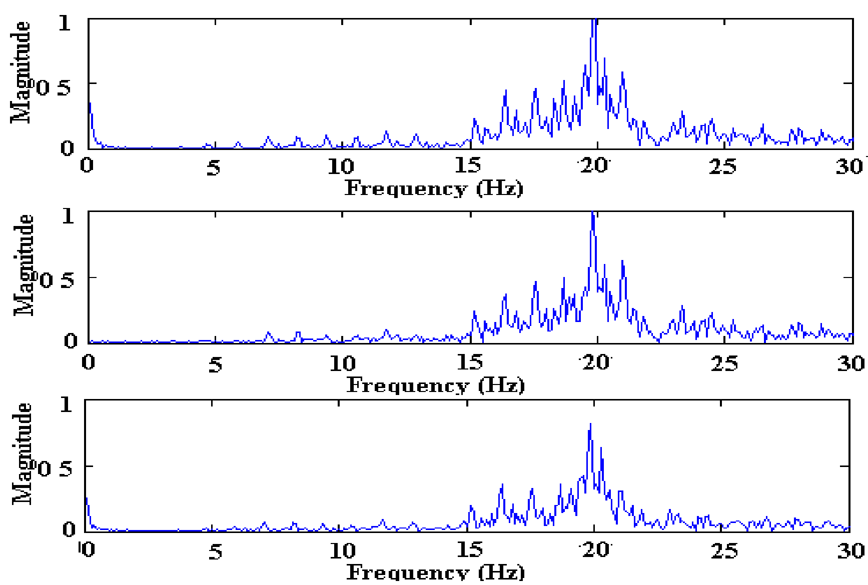

Fig 4.36 Magnitude spectra of pulse waveforms for subject S2_Pr

(a) Before using spectral subtraction

(b) After using spectral subtraction (ABNE)

(c) After using spectral subtraction (QBNE)

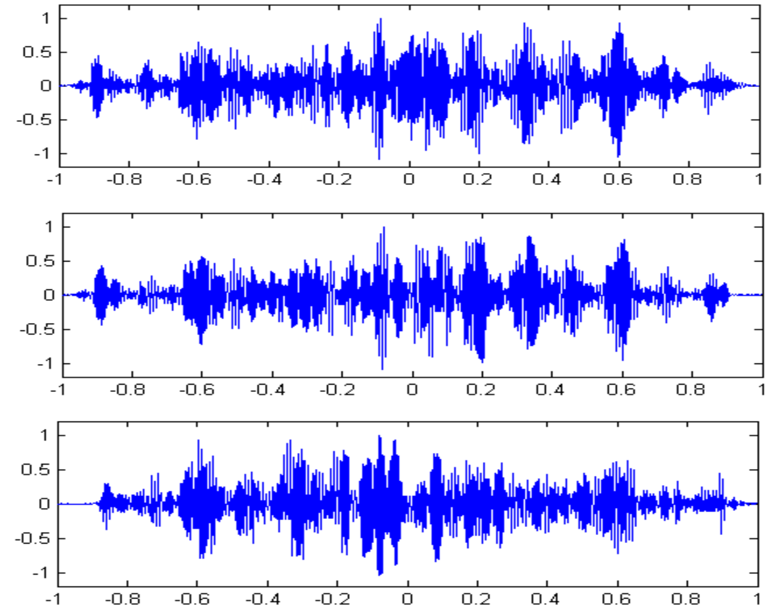

Fig 4.37 Cross-correlation waveform between PCG and pulse waveform for subject S2_Pr

(a) Before using spectral subtraction

(b) After using spectral subtraction (ABNE)

(c) After using spectral subtraction (QBNE)

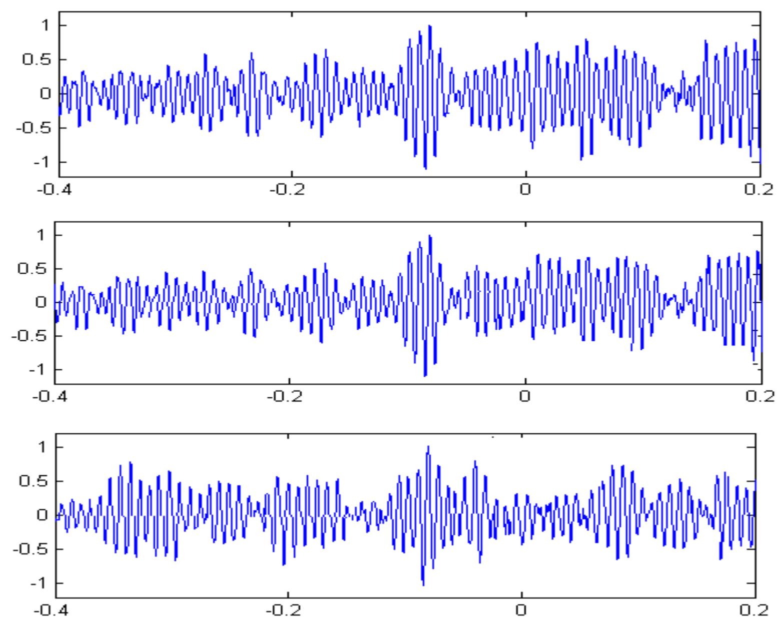

Fig 4.38 Zoomed version of cross-correlation waveform between PCG and pulse signal for subject S2_Pr

Chapter 5

Effect of physical exercise on PCG and pulse waveform

5.1 Introduction

Cross-correlation of pulse waveform with PCG has been investigated for change in the delay in the cross-correlation peak as an indication of change in arterial blood flow rate. The recordings were done for pulse signal and PCG simultaneously by using phonocardiograph as well as the piezoelectric transducer. The subject exercised on an exercise bicycle, so that the pulse rate increased. Recordings were made on normal subjects during the post-exercise relaxation, at different pulse rates until the rate returned to normal. Table 5.1 gives the information about subjects who participated in the recording.

Table 5.1 Subjects' information

Subject code	S1_Ma	S2_Pr	S3_Pi	S4_Ju
Age (years)	30	38	24	24
Sex	M	M	M	F

5.2 Recording with phonocardiograph

The subject S1_Ma exercised on an exercise bicycle, so that the pulse rate became high. During the post-exercise relaxation, PCG was recorded by using transducer Tm and the pulse waveform was obtained by using transducer Ts simultaneously at different pulse rates until it returned to normal. The signal acquisition was done using PC sound card at sampling rate = 11.025 kSa/s and 16-bit, as described earlier in Section 3.2. Fig 5.1 and Fig 5.2 show PCG and pulse waveform respectively obtained at different pulse rates, showing variation in the amplitude with respect to change in the pulse rate. In order to study delay between PCG and pulse waveform as a function of pulse rate, a cross-correlation of the two was computed. Fig 5.3 shows cross-correlation waveforms. Zoomed versions of cross-correlation are shown in Fig 5.4. From Fig 5.4a, the maximum peak of the cross-correlated waveform is obtained at a value of 12.5 ms. It means that the time delay between PCG and pulse waveform, at 116 bpm is 12.5 ms. Similar recordings and analysis were carried out for another subject, S2_Pr. Fig 5.5 shows enhanced pulse after using spectral subtraction with QBNE technique. Cross-correlation between PCG and enhanced pulse waveforms at different pulse rates was computed. Fig 5.6 shows cross-correlation waveforms. Zoomed versions of cross-correlation are shown in Fig 5.7. The location of cross-correlation peak, obtained from cross-correlation between PCG and enhanced pulse is approximately equal to that of between PCG and pulse before using spectral subtraction. The location of cross-correlation peak with respect to the pulse rate during relaxation from exercise is presented in Table 5.2 for two subjects and results are plotted in Fig 5.8.

(a) PCG at 116 bpm

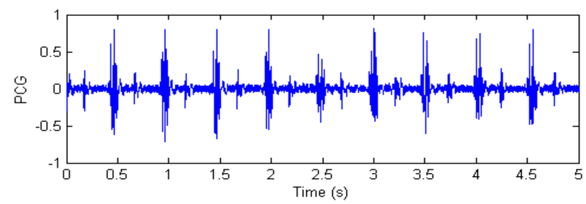

(b) PCG at 114 bpm

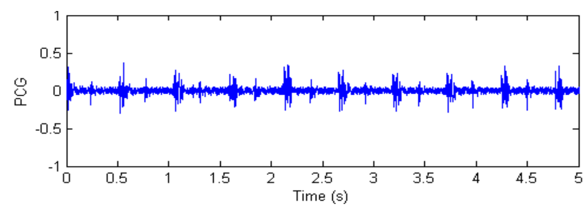

(c) PCG at 108 bpm

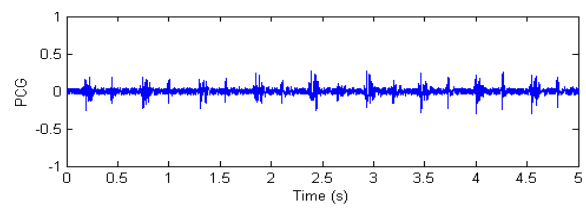

Fig 5.1 PCG at three different pulse rates for subject S1_Ma

(a) Pulse at 116 bpm

(b) Pulse at 114 bpm

(c) Pulse at 108 bpm

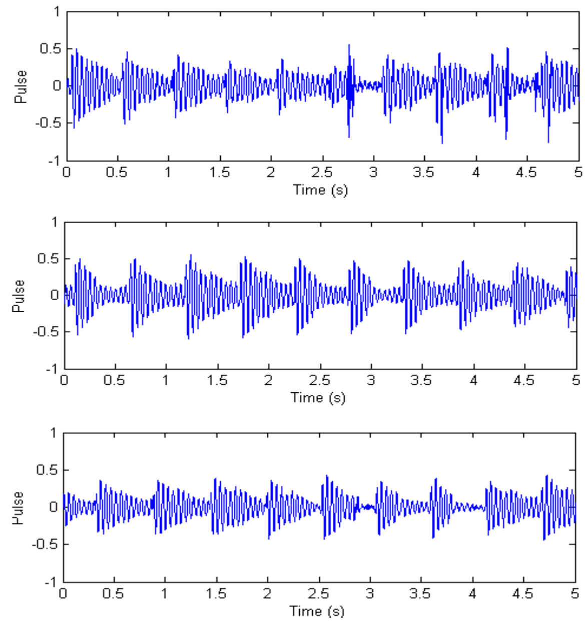

Fig 5.2 Pulse at three different pulse rates for subject S1_Ma

(a) Cross-correlation at 116 bpm

(b) Cross-correlation at 114 bpm

(c) Cross-correlation at 108 bpm

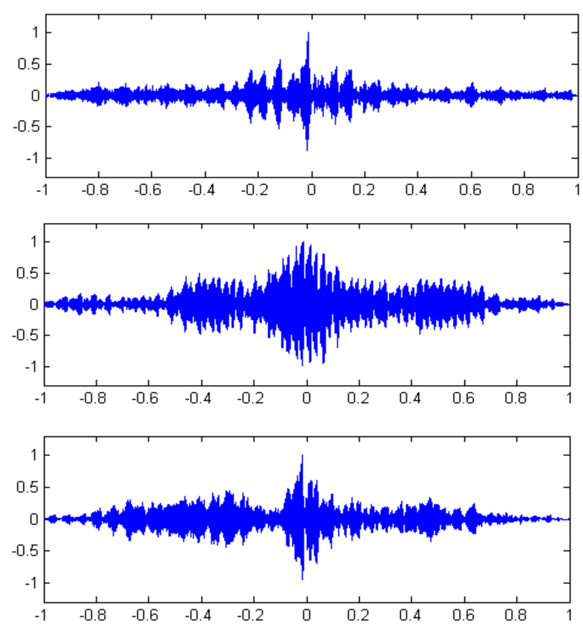

Fig 5.3 Cross-correlation between PCG and pulse at different pulse rates for subject S1_Ma

(a) Zoomed cross-correlation at 116 bpm

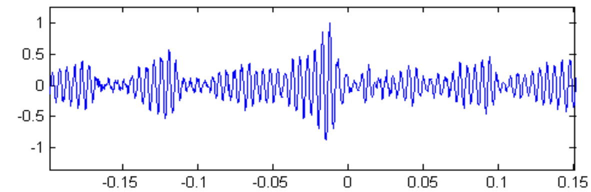

(b) Zoomed cross-correlation at 114 bpm

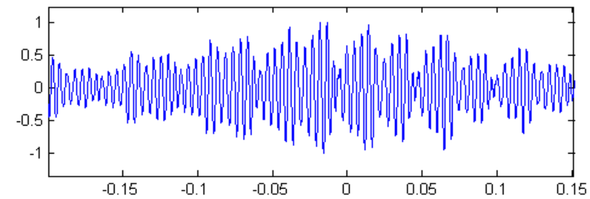

(c) Zoomed cross-correlation at 108 bpm

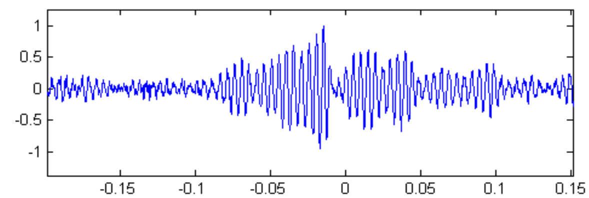

Fig 5.4 Zoomed version of cross-correlation between PCG and pulse at different pulse rates for subject S1_Ma

(a) Enhanced pulse at 116 bpm

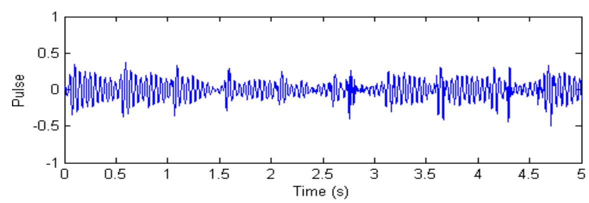

(b) Enhanced pulse at 114 bpm

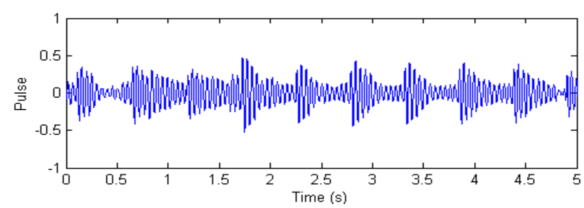

(c) Enhanced pulse at 108 bpm

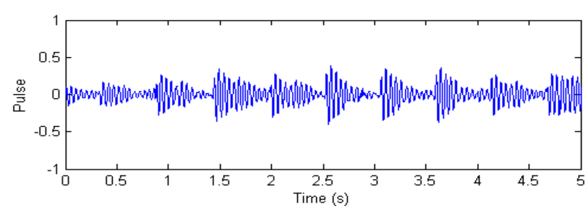

Fig 5.5 Pulse after using spectral subtraction at three different pulse rates for subject S1_Ma

(a) Cross-correlation at 116 bpm

(b) Cross-correlation at 114 bpm

(c) Cross-correlation at 108 bpm

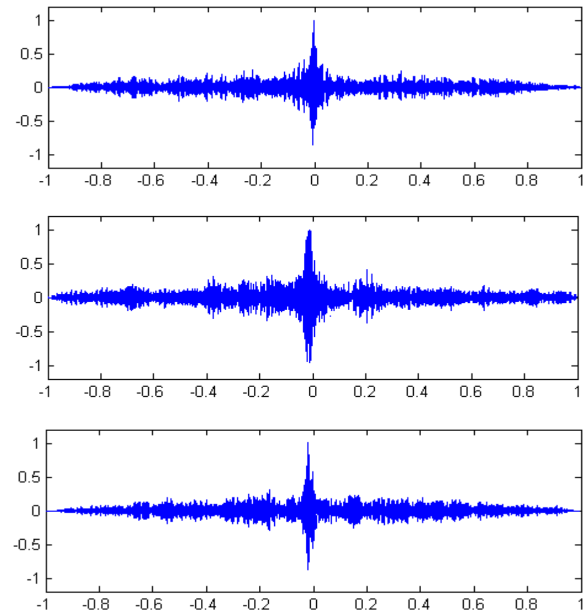

Fig 5.6 Cross-correlation between PCG and enhanced pulse at different pulse rates for subject S1_Ma

(a) Zoomed cross-correlation at 116 bpm

(b) Zoomed cross-correlation at 114bpm

(c) Zoomed cross-correlation at 108 bpm

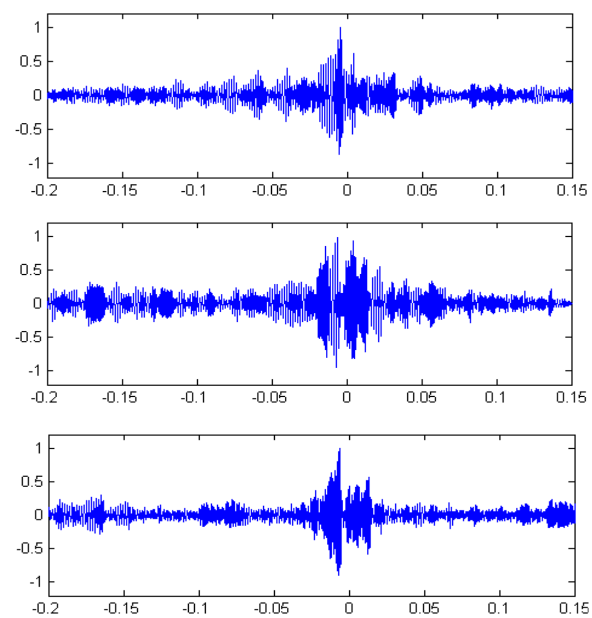

Fig 5.7 Zoomed version of cross-correlation between PCG and enhanced pulse at different pulse rates for subject S1_Ma

Table 5.2 Relation between cross-correlation peak delay and pulse rate during post-exercise relaxation for two subjects S1_Ma, S2_Pr

Subject	Pulse rate (bpm)	116	114	112	110	108
S1_Ma	Delay (ms)	12.5	13.4	13.6	14.3	14.7
Subject	Pulse rate (bpm)	120	110	100	84	76
S2_Pr	Delay (ms)	5	6.2	6.7	7.1	11

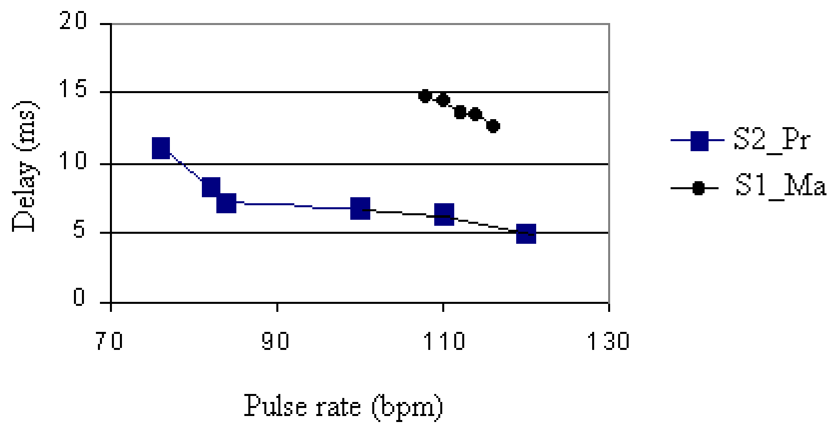

Fig 5.8 Plot of cross-correlation delay vs. pulse rate for results in Table 5.2, for two subjects S1_Ma, S2_Pr

5.3 Recording with piezoelectric transducer

The pulse signal was also acquired by using piezoelectric transducer. The subject exercised to increase the pulse rate. Recordings were made using a DSO (model "Agilent 54621D") with 8-bit quantization and a recording length of 2000 samples, during the post-exercise relaxation at different pulse rates until it returned to normal. The PCG was obtained by using transducer Tm and the pulse waveform was obtained by using piezoelectric transducer. Fig 5.9 shows PCG obtained at different pulse rates for subject S3_Pi. It shows a variation in the amplitude with change in the pulse rate. Pulse waveform obtained at pulse rate from maximum to normal is as shown in Fig 5.10. It also shows a decrease in the magnitude as the pulse rate reduces to normal. In order to study delay between PCG and pulse waveform at corresponding pulse rate, a cross-correlation of the two was computed. Fig 5.11 shows cross-correlation at different pulse rates. Zoomed versions of cross-correlation are shown in Fig 5.12. Similar recordings and analysis were carried out for another subject, S4_Ju. The variation of pulse rate with respect to the pulse rate during relaxation from exercise is presented in Table 5.3 for the two subjects and the results are plotted in Fig 5.13.

(a) PCG at 120 bpm

(b) PCG at 90 bpm

(c) PCG at 66 bpm

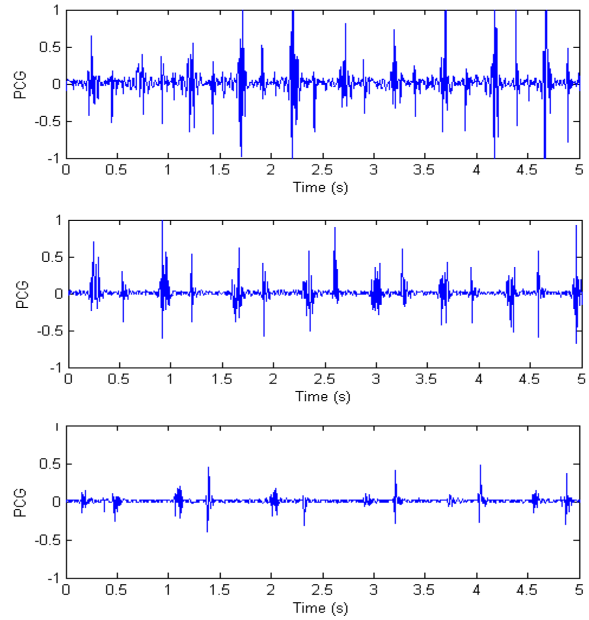

Fig 5.9 PCG at three different pulse rates for subject S3_Pi

(a) Pulse at 120 bpm

(b) Pulse at 90 bpm

(c) Pulse at 66 bpm

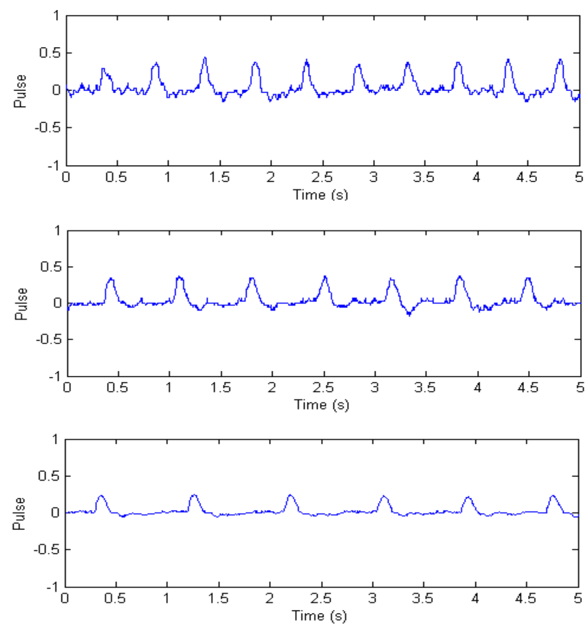

Fig 5.10 Pulse at three different pulse rates for subject S3_Pi

(**a**) Cross-correlation at 120 bpm

(**b**) Cross-correlation at 90 bpm

(**c**) Cross-correlation at 66 bpm

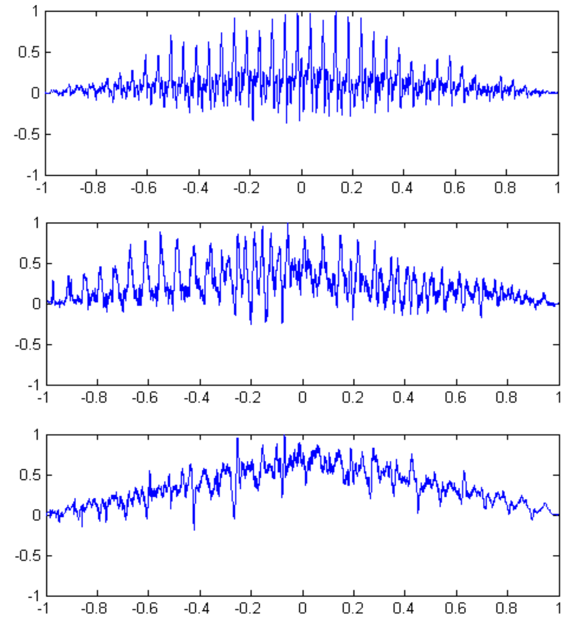

Fig 5.11 Cross-correlation between PCG and pulse at different pulse rates for subject S3_Pi

(**a**) Zoomed cross-correlation at 120 bpm

(**b**) Zoomed cross-correlation at 90 bpm

(**c**) Zoomed cross-correlation at 66 bpm

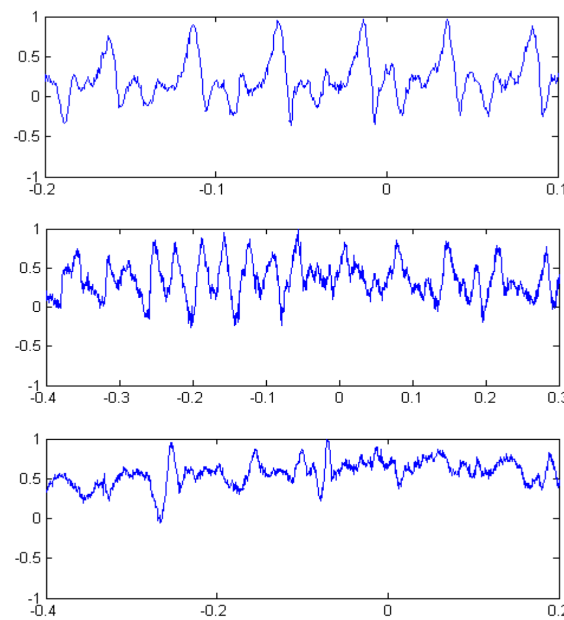

Fig 5.12 Zoomed version of cross-correlation between PCG and pulse at different pulse rates for subject S3_Pi

Table 5.3 Relation between cross-correlation peak delay and pulse rate during post exercise relaxation for S3_Pi, S4_Ju

Subject	Pulse rate (bpm)	120	102	96	84	66
S3_Pi	Delay (ms)	14	15	47	58	70
Subject	Pulse rate (bpm)	102	96	90	84	78
S4_Ju	Delay (ms)	8	12	19	83	97

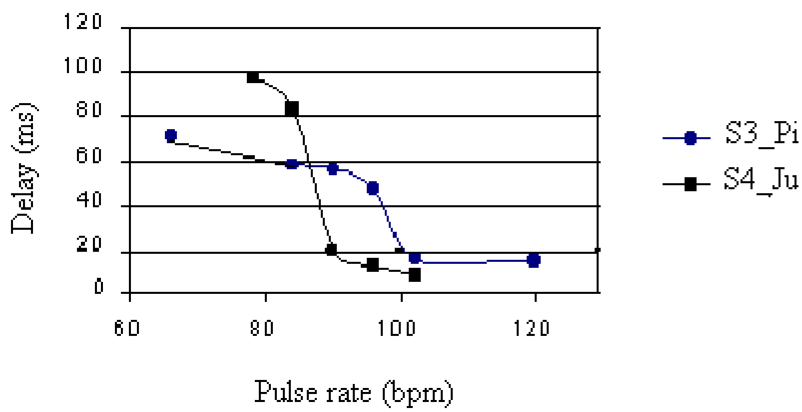

Fig 5.13 Plot of cross-correlation delay vs. pulse rate for results in Table 5.3, for two subjects S3_Pi, S4_Ju

5.4 Discussion

The recordings were done for PCG and the pulse signal simultaneously on several normal subjects by using phonocardiograph as well as the piezoelectric transducer during post exercise relaxation. The variation in delay between PCG and pulse signal was analyzed by obtaining cross-correlation between PCG and pulse signal, at different pulse rates. The plots of pulse rate vs. delay between PCG and pulse signal were obtained. It shows decrease in delay with increase in the pulse rate, indicating an increase in arterial blood flow rate. Study over a large number of subjects and patients may lead in establishing diagnostic information.

Chapter 6

Summary and conclusions

The different sensors used for acquisition of pulse waveform were studied. First, the recording of pulse waveform and PCG from subjects were recorded by using phonocardiographic instruments. The pulse waveform obtained by using the phonocardiograph was corrupted by noise, environmental sounds as well as the vibrations from various smaller blood vessels. Hence signal enhancement techniques were used for obtaining clean pulse waveform for further analysis. As the noise has essentially the same band as the signal, it cannot be effectively reduced by filtering techniques. Spectral subtraction method, reported earlier for enhancement of noisy speech, was investigated for noise reduction in the pulse waveform. For this purpose, estimate of noise spectrum can be obtained using noise recording from a nearby site. The averaged noise spectrum was computed over a certain averaging duration, using a 1.6 s window with 50% overlap. This averaged power spectrum was used for spectral subtraction. The effect of variation of the various parameters used for spectral subtraction was investigated. The effect of optimal averaging duration over which noise estimation is done and site from which noise is recorded were observed for subtraction factor α of 1 and 5. It was found that standard deviation for estimated noise spectrum, decreases with increase in the averaging duration, and effective noise estimation could be done with averaging duration of 16 s. Also the effect of noise site on the PCG was analyzed by using the noise recorded from the chest and noise from the hand, and it was found that for effective enhancement, the noise from a site close to the signal pick-up should be used.

In the earlier method, the noise spectrum was taken to be constant over the entire duration of the signal to be enhanced. An updated estimate of noise spectrum was obtained by use of quantile-based noise estimation technique (QBNE). For this purpose, estimate of noise spectrum was obtained by using a quantile based spectral estimate of noise from the noisy pulse waveform itself. For QBNE, the averaged spectrum of noise from the nearby site was compared with the spectrum of noisy pulse at different quantile values to obtain a set of quantile values for giving a close match. The spectral subtraction was carried out with β=0.001 and varying α over 0.5 to 5. From the results obtained after using noise estimate by averaging and QBNE, it was seen that the value of α and the type of noise estimate both have significant effect on noise reduction as well as over-subtraction. As an estimate of the two, the RMS value of the overall signal and the RMS value of the signal samples in the vicinity of the pulse peaks were calculated. The variation in the RMS values as function of α for the two types of noise estimates was studied which indicated that the best signal enhancement is obtained by using QBNE spectrum for $\alpha \approx 2$.

Further the pulse waveform was acquired by using piezoelectric transducer. The pulse waveform obtained was much less noisy as compared to that by using phonocardiograph sensor. Hence the signal enhancement techniques were not used for the pulse signal picked up using piezoelectric transducer. Analysis of pulse signal can be done in terms of quantitative measurements such as pulse rate, pulse amplitude for more number of subjects. Classification of pulse signal number of healthy as well as diseased subjects can be done on the basis of spectral energy ratio. Simultaneous blood pressure reading can be taken along with the pulse signal at different time instant during whole day, which will help in preparing the clinical database of subject.

The effect of exercise on PCG and pulse waveform, the recordings were done for pulse signal and PCG simultaneously by using phonocardiograph as well as the piezoelectric transducer. Cross-correlation of the pulse waveform with PCG has been investigated for change in the delay in the cross-correlation peak as an indication of change in arterial blood flow rate. The results show that as the pulse rate goes on increasing the delay between PCG and pulse signal decreases, indicating increase in the arterial blood flow rate. Cross-correlation of pulse signal with ECG and impedance cardiograph (ICG) also can be studied. Study of the pulse signal and its cross-correlation with ECG and ICG for a large number of healthy subjects and patients with various cardiovascular disease need to be carried out in order to establish signal analysis technique for obtaining diagnostic information.

Appendix A Sound card specifications

Signal acquisition was carried out using a PC sound card, manufactured by Creative Technology Ltd. The specifications of sound card are given as below [17][18]:

1] *System requirements*	a) Intel Pentium class 90 MHz or 166 MHz computer with PCI slot for Windows NT 4.0 and Windows 95. b) 16 MB RAM for Windows NT 4.0 and 64 MB RAM for Windows 2000
2] *Analog input port characteristics*	Analog input is a sum obtained through an internal mixer from two analog inputs: a) Microphone (Mic) powered by 2.5 V supply from sound card b) Line-in with voltage range of 0-9V and input impedance of 53kΩ at 1 kHz Bandwidth: 10 Hz to fs/2 Hz
3] *Output*	a) Speaker Out/Line Out connects non-powered speaker by default with output impedance of 0.767Ω at 1 kHz with 4 watts per channel for 4 Ω stereo output. Also connects powered speaker and an external amplifier when built-in amplifier is disabled by changing jumper setting on the sound card.
4] *Digitization*	a) For analog input: Sampling rate = 11025, 22050, or 44100 sa/s No. of quantization bits = 8 or 16 b) For analog output: Sampling rate = settable to a value in the range of 5000 Hz to 44100 Hz No. of quantization bits = at 8 or 16

Appendix B Significance of cross-correlation

The objective in computing correlation between the two signals is to measure the degree to which the two signals are similar. The cross-correlation between two signal sequences $x(n)$ and $y(n)$ is a sequence $r_{xy}(l)$, which is defined as [25]

$$r_{xy}(l) = \sum_{n=-\infty}^{\infty} x(n)y(n-l) \qquad l = 0, \pm 1, \pm 2, \ldots \tag{1}$$

or, equivalently, as

$$r_{xy}(l) = \sum_{n=-\infty}^{\infty} x(n+l)y(n) \qquad l = 0, \pm 1, \pm 2, \ldots \tag{2}$$

If the two sequences are totally uncorrelated, the cross-correlation will have a low value for all 'l' . In case both waveforms have the same signal as the strong constituent, the delay for which maximum peak of cross-correlation occurs indicates the delay between the two sequences.

The cross-correlation of $x(n)$ and its delayed version $x(n+d)$ yield a result that has a peak at n = -*d*. From Fig A.1 and A.2, it is clear that the cross-correlation between the unshifted PCG and right shifted PCG gives the maximum peak at negative value. However, the cross-correlation of $x(n)$ and its delayed version $x(n-d)$ yield a result that has a peak at n = *d*. The cross-correlation between unshifted PCG and left shifted PCG gives maximum peak at positive value, as shown in Fig A.3 and A.4.

(a) PCG

(b) Right shifted PCG, delay = 0.9 s

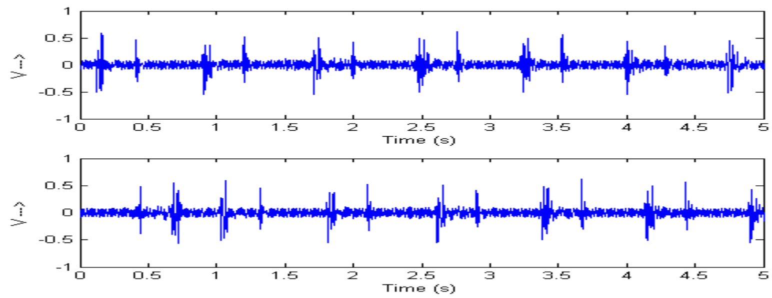

Fig A.1 PCG and right shifted PCG

(a) Cross-correlation

(b) Zoomed version

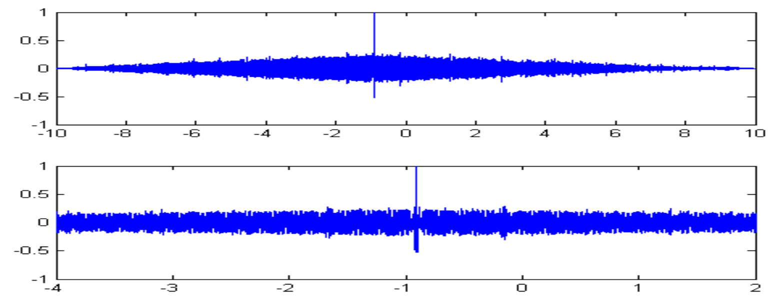

Fig A.2 Cross-correlation between PCG and right shifted PCG

(a) PCG

(b) Left shifted PCG, advancement = 0.9 s

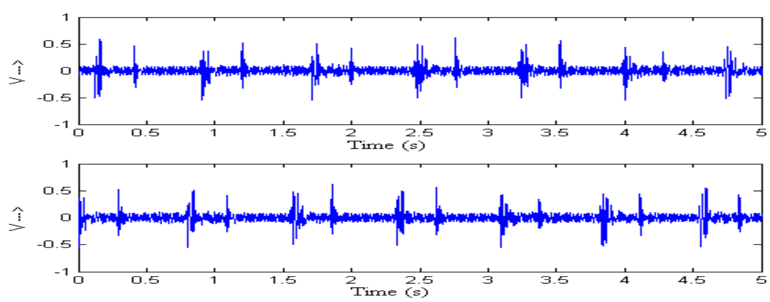

Fig A.3 PCG and left shifted PCG

(a) Cross-correlation

(b) Zoomed version

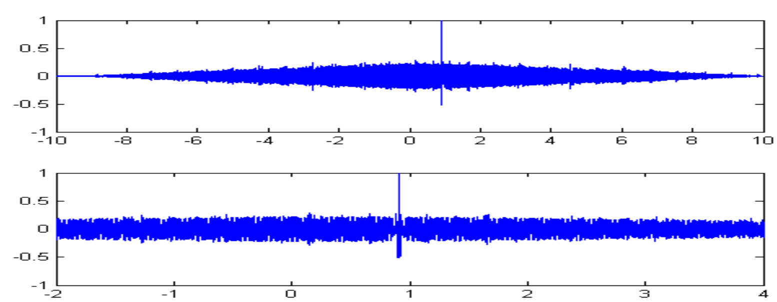

Fig A.4 Cross-correlation between PCG and left shifted PCG

References

1. P. Pandit, *Nadividnyanam* (Sanskrit), Varanasi: Chaukhamba Sanskrit Series, 1954, pp. 2-35.
2. A. Pandey, *Nadirahasya* (Hindi), Varanasi: Medical Pustak Bhavan, 1956, pp. 5-22.
3. S. Upadhyay, *Nadi Vijnana* (*Ancient pulse science*), Varanasi: Chaukhamba Sanskrit Series, 1986, pp. 162-163.
4. "Dudgeon' s sphygmograph," website of University of Iowa Health Care, Iowa City, Iowa, http://www.uihealthcare.com/depts/medmuseum/gallaeryexhibits/ beatgoesonhistory/02bloodpressre.html, accessed in 2001.
5. J. Webster, *Encyclopedia of Medical Devices and Instrumentation*, New York: Wiley, 1988, pp. 2770-2776.
6. M. Dasrao, Y. Hock, and E. Sim, "Diagnostic blood pressure wave analysis and ambulatory monitoring using a novel, non-invasive portal device," *Proceedings of International Conf. on Biomedical Engineering Biovision 2001*, 2001, pp. 267-272.
7. "MediWatch," website of HealthSTATS International Pte Ltd, Singapore, http:// www.heathstats.com.sg, accessed in 2004.
8. "Arterial Tonometry," website of Colin Europe, Courbevoie, France, http:// www. colin-europe.com/pages/tonometry.html, accessed in 2004.
9. W. Binghe and X. Jinglin, "Detecting system and power-spectral analysis of pulse signals of human body," *Proceedings of International Conf. on Signal Processing*, Beijing, China, 1998, pp. 1646-1649.
10. G. Pressman and P. Newgard, "A transducer for the continuous external measurement of arterial blood pressure," *IEEE Trans. Biomedical Engineering*, vol. BME 10, 1963, pp. 73-81.
11. S. Shah/ Prof. T. Anjaneyulu (Supervisor), "Blood pressure measurement," *M. Tech. Dissertation*, EE Dept., IIT Bombay, 1977.
12. C. Lee and L. Wei, "Spectrum analysis of human pulse," *IEEE Transaction of Biomedical Engineering*, vol. BME-30, 1983, pp. 348-352.

13. L. Wei and P. Chow, "Frequency distribution of human pulse spectra," *IEEE Transaction of Biomedical Engineering*, vol. BME-32, 1985, pp. 245-246.
14. R. S. Khandpur, *Handbook of Biomedical Instrumentation*, New Delhi: McGraw-Hill, 1987, pp.106-108.
15. J. Webster, *Medical Instrumentation: Application and Design*, New York: Wiley, 1998, pp. 311-312.
16. "Stethmate Electronic Stethoscope," website of Electronic Engineering Corporation, Tamilnadu, India, http://www.eeconnet.com/stethmate.htm, accessed in 2004.
17. *Sound Blaster 16 Manual*, Creative Technologies Ltd., 1997.
18. "Creative Sound Blaster AudioPCI card," website of University of Waterloo, Waterloo, Ontario Canada, www.eng.uwaterloo.ca/cphmmlab/assets/manuals/ Classroom%20Computer/ sb16pci.pdf, accessed in 2004.
19. M. Berouti, R. Schwartz and J. Makhoul, "Enhancement of speech corrupted by acoustic noise," *Proc. IEEE. Conf. on Acoust. Speech Signal Processing*, 1979, pp. 208-211.
20. R. W. Schafer and J. D. Markel, *Speech Analysis,* New York: IEEE Press, 1979, pp. 153.
21. S. Boll, "Suppression of acoustic noise in speech using spectral subtraction," *IEEE Trans. ASSP*, vol. ASSP-27, 1979, pp. 113-120.
22. P. C. Pandey, S. M. Bhandarkar, G. Bachher, and P. K. Lehana, "Enhancement of alaryngeal speech using spectral subtraction," *Proc. 14th Int. Conf. on Digital Signal Processing DSP 2002*, 2002, pp. 591-594.
23. S. S. Pratapwar, P. C. Pandey, and P. K. Lehana, "Reduction of background noise in alaryngeal speech using spectral subtraction with quantile based noise estimation," *Proc. of 7th World Multiconference on Systemics, Cybernetics and Informatics SCI* 2003, 2003.
24. V. Stahl, A. Fischer, and R. Bippus, "Quantile based noise estimation for spectral subtraction and Wiener filtering," *Proc. ICASSP '00*, 2000, pp. 1875-1878.
25. J. Proakis and D. Manolakis, *Digital Signal Processing*: *Principles*, *Algorithms and Applications*, New Delhi: Prentice-Hall, 2000, pp.120-121.

Publication by the candidate

Aparna M. Surve, Prem C. Pandey, S. S. Pratapwar, Vinod K. Pandey, and N.S. Manigandan "Enhancement of radial arterial pulse waveform by spectral subtraction", In Proc. of Inter. Conf. on Systemics, Cybernetics and Informatics (ICSCI-2004, Hyderabad), Feb. 12-15, 2004, pp.323-326.

ENHANCEMENT OF RADIAL ARTERIAL PULSE BY SPECTRAL SUBTRACTION

Aparna M. Surve
EE Dept., IIT Bombay
Powai, Mumbai 400 076, India
(+91-22) 2576 4417
aparnas@ee.iitb.ac.in

Prem C. Pandey
S.S. Pratapwar
EE Dept., IIT Bombay
Powai, Mumbai 400 076, India
(+91-22) 2576 7445
pcpandey@ee.iitb.ac.in
santosh@ee.iitb.ac.in

Vinod K. Pandey
N.S. Manigandan
Bio School, IIT Bombay
Powai, Mumbai 400 076, India
(+91-22) 2576 4417
vinod@ee.iitb.ac.in
manigandanns@iitb.ac.in

ABSTRACT
Noninvasive recording of pressure pulse waveform from the radial artery can be used for obtaining valuable diagnostic information, by analyzing it for temporal characteristics, spectral characteristics, and its cross-correlation with phonocardiogram and ECG. The pulse waveform can be recorded using the transducer of an electronic stethoscope, but the signal is corrupted by noise. We have investigated the use of spectral subtraction method, reported earlier for enhancement of noisy speech, for noise reduction in the pulse waveform. Enhancement can be carried out by taking the noise recording from a nearby site, or by using a quantile based spectral estimate of noise from the noisy pulse waveform.

Keywords
Signal enhancement, radial arterial pulse, spectral subtraction.

1. INTRODUCTION
In most traditional systems of medicine, e.g. *nadisastra* (a branch of *ayurveda*, ancient and well established medical system of India), sensing of arterial pulse pressure forms an essential part of diagnosis. Normally physician's palm supports the patient's wrist and pulse examination is done using finger tips [11]. The diagnosis requires a long period of study and practice by the individual physician, without the benefit of any physical recordings and analysis aids. Lately several investigations have been reported on noninvasive recording and analysis of arterial pressure pulse waveform [3,5,7].

Paper Identification Number: CI-1.7

This paper has been published by the Pentagram Research Centre (P) Limited. Responsibility of contents of this paper rests upon the authors and not upon Pentagram Research Centre (P) Limited. Individual copies could be had by writing to the company for a cost.

Analysis of the waveform for its temporal and spectral characteristics can give valuable diagnostic information, particularly when used together with electrocardiogram (ECG) and phonocardiogram (PCG). Cross-correlation of arterial pulse with ECG and PCG waveforms may provide important diagnostic information about arterial blood flow.

Early studies on pulse waveform have used Dudgeon's sphygmograph [6,11]. Its use involved a tedious process of preparation of tracings and measurements from the tracings. Further, it had other limitations like poor dynamic response. Several instruments have been developed and reported for sensing the pulse waveform and giving the output as electrical analog voltage or as digitized samples and built-in analysis [1,3,5,7]. The arterial tonometer is one such instrument for acquisition of beat-to-beat blood pressure waveform along with numerical values for systolic, mean, diastolic pressure and pulse rate [1].

The pulse waveform can be recorded using the transducer of an electronic stethoscope or phonocardiograph. The main advantage of this technique is a good dynamic response. But the signal is corrupted by noise, environmental sounds as well as the vibrations from various smaller blood vessels. As the noise has essentially the same band as the signal, it cannot be reduced by filtering techniques. We have investigated the use of spectral subtraction method, reported earlier for enhancement of noisy speech, for noise reduction in the pulse waveform. For this purpose, estimate of noise spectrum can be obtained using noise recording from a nearby site or by using a quantile based spectral estimate of noise from the noisy pulse waveform itself.

2. SPECTRAL SUBTRACTION ALGORITHM
The basic assumption in spectral subtraction method [2,4,8], developed for enhancement of speech corrupted by noise, is that the clean signal and the noise are uncorrelated, and therefore the power spectrum of noisy signal equals the sum of power spectrum of noise and clean signal. Let $x(n)$ be the windowed noisy signal comprising of the clean signal $s(n)$ and the additive noise $l(n)$,

$$x(n) = s(n) + l(n) \tag{1}$$

Taking short-time Fourier transform on both sides, we get

$$X_n\left(e^{jw}\right) = S_n\left(e^{jw}\right) + L_n\left(e^{jw}\right) \tag{2}$$

Assuming $s(n)$ and $l(n)$ to be uncorrelated, we get

$$\left|X_n\left(e^{jw}\right)\right|^2 = \left|S_n\left(e^{jw}\right)\right|^2 + \left|L_n\left(e^{jw}\right)\right|^2 \tag{3}$$

The basic spectral subtraction algorithm works in two steps: (i) noise spectrum is estimated and (ii) the estimated noise spectrum is subtracted from that of the noisy signal to get

$$\left|Y_n\left(e^{jw}\right)\right|^2 = \left|X_n\left(e^{jw}\right)\right|^2 - \left|L_n\left(e^{jw}\right)\right|^2 \tag{4}$$

The resulting magnitude spectrum is then combined with the original phase spectrum to resynthesize the "cleaned" signal. Using FFT for implementation, the steps can be written as

$$|Y_n(k)|^2 = |X_n(k)|^2 - |L(k)|^2 \tag{5}$$

$$y_n(m) = IFFT\left[|Y_n\ k|\, e^{j\angle X_n(k)}\right] \tag{6}$$

When the estimate of the noise spectrum is subtracted from the actual noise spectrum, all the spectral peaks are shifted down while the points lower than the estimate are set to zero. Hence, after subtraction, noise spectrum is obtained with peaks. The wider peaks are considered as a broadband noise and the narrower peaks are considered as the musical noise. Thus the spectral subtraction method is modified for minimizing this noise [2].

$$|Y_n(k)|^2 = |X_n(k)|^2 - \alpha|L(k)|^2$$

$$|Y'_n(k)|^2 = |Y_n(k)|^2 \qquad \text{if } |Y_n(k)|^2 > \beta|L(k)|^2$$

$$= \beta|L(k)|^2 \qquad \text{otherwise} \tag{7}$$

where α is the subtraction factor and β is the spectral floor factor.

A block diagram of the modified spectral subtraction algorithm is shown in Figure 1.

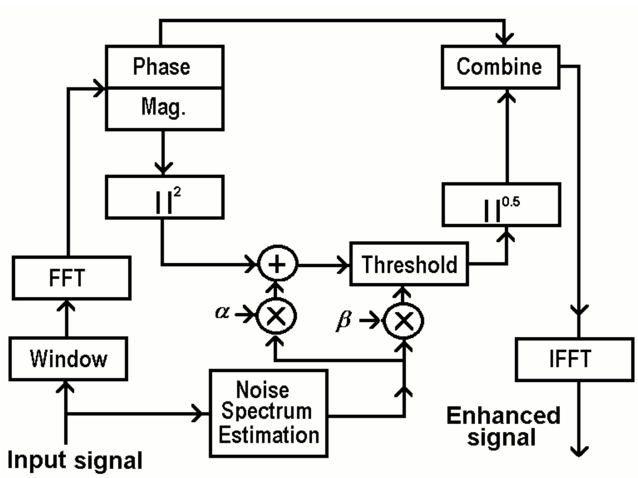

Figure 1: Spectral subtraction algorithm [8].

With $\alpha > 1$, the noise will be over subtracted from the noisy signal. However over subtraction increases signal distortion. This is taken care by the spectral floor factor β. The spectral components of $|Y'_n(k)|^2$ are prevented from going below $\beta|L(k)|^2$. The implementation via FFT requires overlap-and-add in order to prevent discontinuities at frame boundaries [2].

For enhancement of noisy speech signal, a speech / non-speech detection is used for updating the noise estimate. In case of arterial pressure pulse waveform, the signal and corrupting noise both are always present. Assuming that the noise is stationary, its average spectrum can be estimated from the noise recorded from a nearby site, which does not show the pulse waveform. Recently, techniques for speech enhancement without involving speech / nonspeech detection have been reported [9,10]. These are based on quantile analysis of the signal spectrum. This method can be used for noise estimation for enhancement of pulse waveform for dynamic tracking of variations in noise spectrum.

3. NOISE ESTIMATION

The pulse waveforms were recorded by keeping PCG sensor over radial artery on the wrist and adjusting the position for strongest signal pick up. The noise was acquired by keeping the sensor on the same hand but away from the radial artery at two different locations. The waveforms were acquired using PC sound card with a sampling rate of 1.1,025 k sa/s (11.025 k Sa/s, followed by 10:1 decimation). The averaged noise spectrum was computed over a record of 16 s, using a 1.6 s window with 50% overlap. This averaged power spectrum is used for spectral subtraction.

In the above method, the noise spectrum is taken to be constant over the entire duration of the signal to be enhanced. An updated estimate of noise spectrum can be obtained by use of quantile-based noise estimation (QBNE) technique [9,10]. It is based on the assumption that frequency bins in the signal spectrum tend not to be permanently occupied. The noisy pulse signal is analyzed on a frame-by-frame basis, to obtain an array of the power spectral values for each frequency sample, for a certain number of frames. Then the magnitude-squared values in this array are sorted for obtaining a particular quantile value. The power spectrum of noisy pulse at different quantile values is compared with the mean power spectrum of noise recorded from the nearby site for obtaining the quantiles in frequency bands for matching the two spectra.

4. RESULTS

Spectral subtraction algorithm was used for enhancement of radial arterial pulse obtained from the analog electrical output of an electonic stethoscope (Stethmate). The effect of noise recorded at several sites on the same hand was studied. Fig. 2 shows the noisy pulse waveform and noise obtained at two different locations on hand. Spectral subtraction was carried out with β=0.001 and varying α over 0.5 to 5. It was seen that lower values of α did not result in good noise subtraction, while larger values resulted in over-subtraction and a reduction in pulse peaks. Fig.3 shows an example of pulse waveform after spectral subtraction.

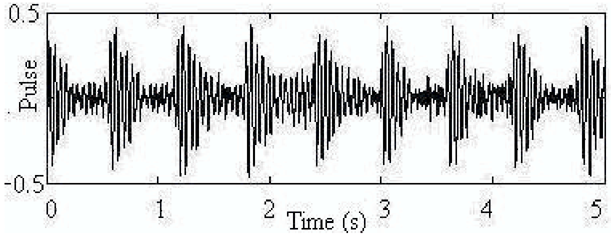

(a)

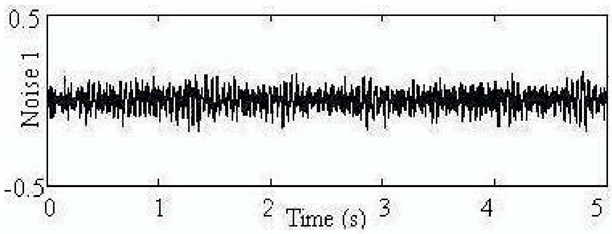

(b)

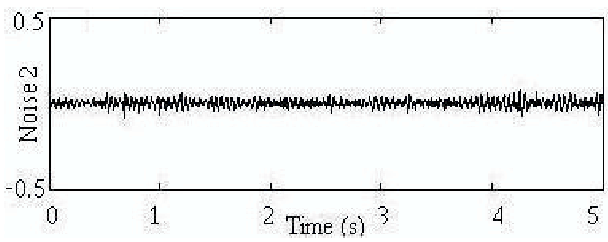

(c)

Figure 2: Pulse pressure waveform: (a) noisy pulse waveform (b) noise at location 1 (c) noise at location 2.

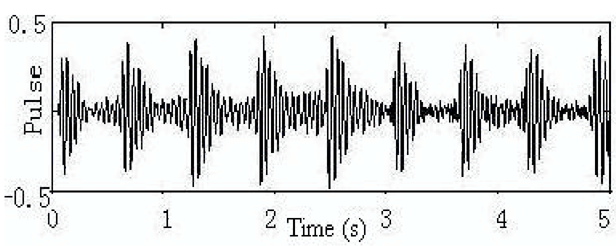

Figure 3: Enhanced pulse waveform by using noise estimation from noise recorded at location 1, using α =2.

For QBNE, the averaged spectrum of noise from the nearby site was compared with the spectrum of noisy pulse at different quantile values to obtain set of quantile values for giving a close match. It was observed that a good match could be obtained for 5 percentile for frequencies less than 32 Hz and 70 percentile for higher frequencies. Fig. 4 shows the averaged spectrum of noise and two quantile based estimates. Fig. 5 shows an example of pulse waveform enhanced using QBNE spectrum.

It was seen that the value of α and the type of noise estimate both have significant effect on noise reduction as well as over-subtraction. As an estimate of the two, the RMS value of the overall signal and the RMS value of the signal samples in the vicinity of the pulse peaks were calculated. Fig. 6 shows a plot of these RMS values as function of α for the two types of noise estimates. It is seen that for averaged noise estimate, both the RMS values decrease with increasing α. For QBNE spectrum, the noise estimation is much more effective. For $\alpha > 2$, the peak RMS decreases without any further decrease in signal RMS. Hence we can say that, we get the best signal enhancement by using QBNE spectrum for $\alpha \approx 2$.

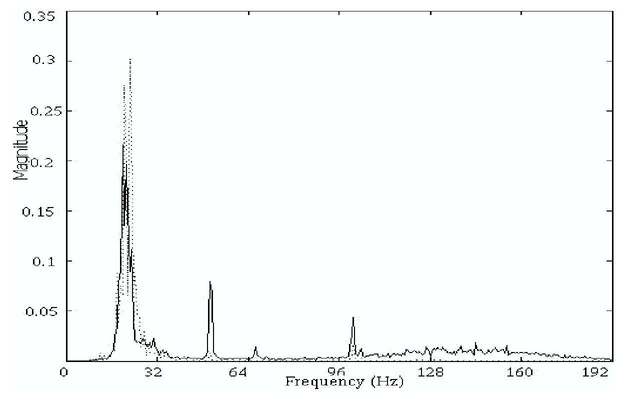

(a)

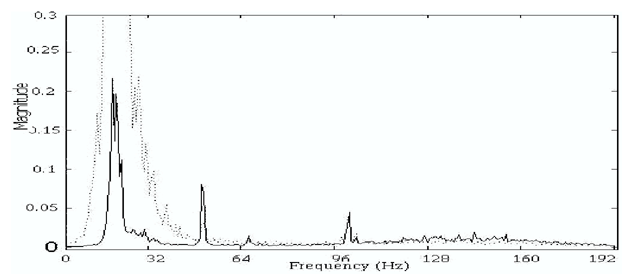

(b)

Figure 4: Averaged noise spectrum and QBNE spectrum for (a) 5 percentile and (b) 70 percentile. Plot with solid line shows the average power spectrum of noise and the plot with dotted line shows the quantile derived spectrum of noisy pulse.

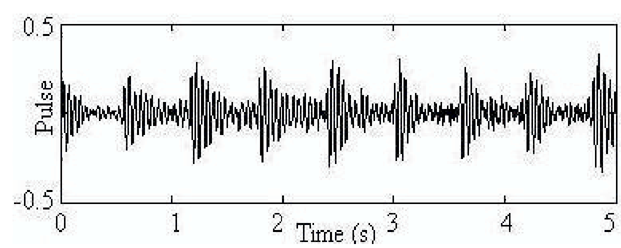

Figure 5: Enhanced pulse waveform by using noise estimation from noisy pulse using QBNE, using α =2.

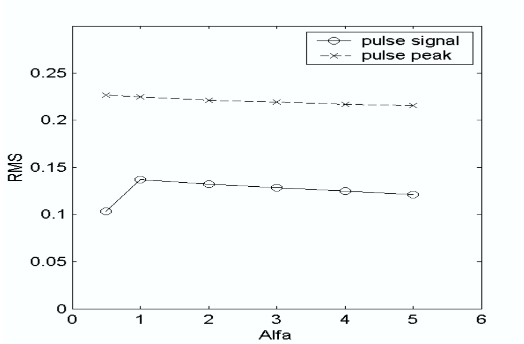

(a)

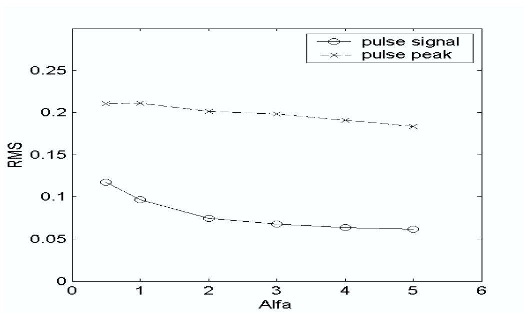

(b)

Figure 6: Effect of α on reduction of noise and peak (a) with averaged noise spectrum and (b) with QBNE.

5. CONCLUSION

Spectral subtraction, reported earlier for enhancement of noisy speech, has been investigated for enhancement of arterial pulse pressure waveform recorded using PCG transducer. It is seen that a quantile based estimation of the noise spectrum from the noisy pulse itself can be used. We are carrying out further study of cross-correlation of the enhanced pulse waveform with simultaneously recorded PCG and ECG waveforms, for possible diagnostic applications.

6. REFERENCES

[1] Arterial Tonometry, http://www.colin- europe.com/pages/ tonometry.html, (2002).

[2] Berouti, M., Schwartz, R., and Makhoul, J. Enhancement of speech corrupted by acoustic noise. In Proc. ICASSP ’79, (1979), 208-211.

[3] Binghe, W., and Jinglin, X. Detecting system and power spectral analysis of pulse signals. In Proc. of ICSP '98, (1998), 1646-1649.

[4] Boll, S. F. Suppression of acoustic noise in speech using spectral subtraction. IEEE Trans. ASSP, 27, 2, (1979), 113-120.

[5] Dasrao, M. S., Hock, Y. J., Sim, E. K. W. Diagnostic blood pressure wave analysis and ambulatory monitoring using a novel non-invasive portable device. In Proc. Int. Conf. Biomedical Engineering Biovision 2001, (Bangalore, 2001), 267-272.

[6] Dudgeon's sphygmograph, http://www.uihealthcare.com/ depts/medmuseum/galleryexhibits/beatgeohistory/ 02bloodpressue.html, (2001).

[7] Lee, C., and Wei, L. Spectrum analysis of human pulse. IEEE Trans. Biomedical Engineering, 30, (1983), 348-352.

[8] Pandey, P. C., Bhandarkar, S. M., Bachher, G. K., and Lehana, P. K. Enhancement of alaryngeal speech using spectral subtraction. In Proc. 14th Int. Conf. on Digital Signal Processing DSP 2002, (Santorini, Greece, 2002), 591-594.

[9] Pratapwar, S. S., Pandey, P. C., and Lehana, P. K. Reduction of background noise in alaryngeal speech using spectral subtraction with quantile based noise estimation. In Proc. of 7th World Multiconference on Systemics, Cybernetics and Informatics SCI, (Orlando, USA, 2003).

[10] Stahl, V., Fischer, A., and Bippus, R. Quantile based noise estimation for spectral subtraction and Wiener filtering. In Proc. ICASSP '00, (2000), 1875-1878.

[11] Upadhyay, S. Nadi Vijnana : Ancient Pulse Science. Chaukhamba Sanskrit Series, Varanasi, 1986.